Aus dem Fachbereich Medizin

der Johann Wolfgang Goethe-Universität

Frankfurt am Main

betreut am

Zentrum der Chirurgie

Klinik für

Mund-, Kiefer- und Plastische Gesichtschirurgie

Direktor : Prof. Dr. Dr. Dr. Robert Sader

Ex vivo and in vivo analysis of tissue reaction
towards collagen membrane (Symbios)

Dissertation

zur Erlangung des Doktorgrades der Medizin

der Johann Wolfgang Goethe-Universität

Frankfurt am Main

vorgelegt von

Chakorn Vorakulpipat

aus Bangkok (Thailand)

Frankfurt am Main, 2018

Dekan:	Prof. Dr. Josef M. Pfeilschifter
Referent:	Prof. Dr. Dr. Dr. Shahram Ghanaati
Korreferent:	Prof.Dr. Johannes Frank
Tag der mündlichen Prüfung:	20.11.2019

Table of Contents

List of abbreviations

BM   Biomaterial

BSE   Bovine spongiform encephalopathy

CD (-molecule)   Cluster of differentiation (distinguishing groups)

CD68   Cluster of differentiation 68, surface protein on human
                      monocytes and macrophages

EDTA   Ethylenediaminetetraacetic acid

g   Gram

GBR   Guided bone regeneration

GTR   Guided tissue regeneration

H&E   Hematoxylin and Eosin stains

IgG   Immunoglobulin G

IL-1   Interleukin-1

i-PRF   Injectable platelet-rich fibrin

M   Meter

mm   Millimeter

mm^2 Square millimeters

MNGCs   Multinucleated giant cells

PRF   Platelet-rich fibrin

PTFE   Polytetrafluorethylen

RCF   Relative centrifugal forces

SB   SYMBIOS® Collagen Membrane SR

TBS   Tris Buffered Saline Wash Solution

TGF-ß1	Transforming growth factor-beta 1
TRAP	Tartrate-resistant acid phosphatase
VEGF	Vascular endothelial growth factor
μm	Micrometer
ZFE	The Animal welfare officer and central facility

Illustration directory

Table

Figure

Diagram

1. Introduction

In the field of maxillofacial and oral surgery, bone regeneration has been a challenging condition to manage [1]. In addition to bone atrophy after tooth loss, surgical treatment of intra- or extraorally located benign and malignant tumors, for instance, is one of the causative factors of significant tooth and bone loss [2]. The alveolar ridges are continuously reduced after tooth loss, consequently decreasing the quantity, altering the quality, and adapting the form and biology of an atrophic bone [3,4]. and patients may greatly benefit from dental implant placement as part of their oral rehabilitation. However, in these cases, dental implant placement often requires bone tissue regeneration in the form of bone augmentation to generate a sufficient implantation bed [5,6].

Therefore, guided bone regeneration (GBR), which is a surgical concept that involves the use of barrier membranes to promote bone regeneration in combination with bone grafts or bone substitutes has become widely established. Successful bone regeneration is based on the presence of two cellular components in the tissue: slow-migrating osteoblasts and the rapidly proliferating cells (fibroblasts and other soft connective-tissue cells) [7,8]. In GBR, a mechanical interference, i.e., a membrane, serves as a barrier to hinder the more rapidly proliferating epithelium and connective tissue ingrowth and to maintain space for new bone formation, which requires a longer period [7–11].

1.1. Scientific Background

1.1.1. bone atrophy

Following tooth removal, the alveolar process undergoes atrophy due to the lack of force transmission on the jawbone during the chewing process. Vertical and horizontal resorption of the alveolar bone occurs, progressing in the centripetal direction in the upper jaw and in the centrifugal direction in the lower jaw [12,13].

Together with the lack of loading and unloading forces through the periodontium, as well as the presence of force on the edentulous ridge from the lip, cheek and tongue, other factors that may affect the speed and direction of jaw atrophy include the design and location of the prosthetic restoration, age and sex, and hormonal imbalances or inflammatory processes [14].

The factors influencing bone atrophy include the following [14]:

☐ Age

☐ Sex

☐ Upper or lower jaw

☐ The degree of pneumatization in the maxillary sinus

☐ Bone density

☐ Hormonal control of bone metabolism

☐ A history of periodontal disease and inflammation of the alveolar process

☐ Nonphysiological pressure loading due to mucous membrane-supported dentures

The rate of bone resorption and the progression of alveolar ridge atrophy are subject to individual fluctuations, but in general, the most significantly changes are observed in the first year after tooth removal [15].

Bone resorption in the lower jaw involves up to four times higher atrophy than bone resorption in the upper jaw. The main reason for this difference may be the pressure load of the alveolar bone in the upper jaw, which is higher than that in the lower jaw due to the presence of a larger denture base compared to the lower jaw. [16]

Staging	Alveolar bone morphology
Class I	Dentate
Class II	Immediately post extraction
Class III	Well-rounded ridge form
Class IV	Knife-edge ridge form, adequate in height but inadequate in width
Class V	Flat ridge form, inadequate in height and width
Class VI	Depress ridge form, width some basalar loss evident.

Table 1: Classification of the edentulous jaws [13, 17]
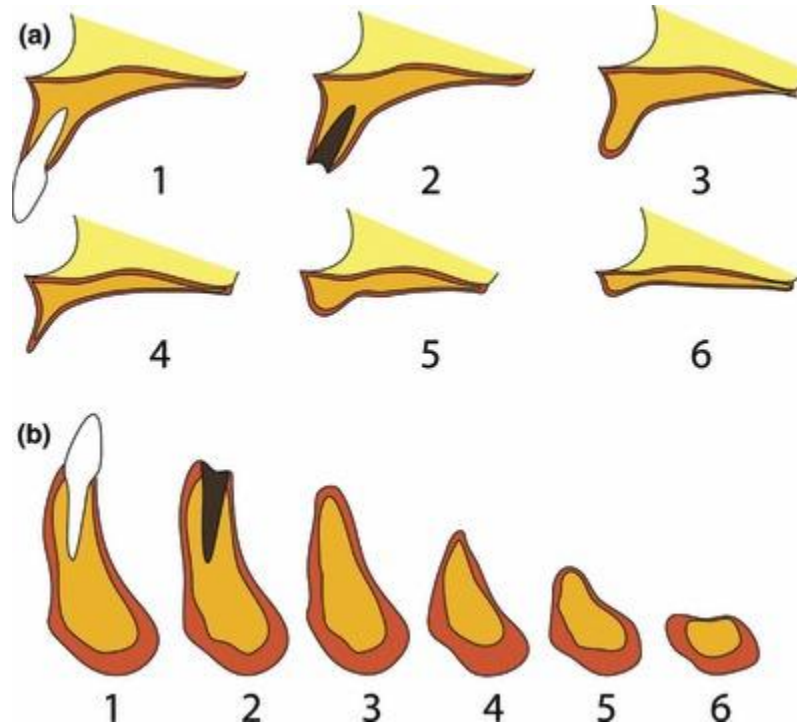
Figure 1: Classification system of six atrophy stages in the maxilla (a) and the mandible (b), according to Atwood (1963) and Cawood and Howell (1988). Atrophy stage 1: pre-extraction, stage 2: post-extraction, stage 3: high, well-rounded ridge, stage 4: knife-edge shaped ridge, stage 5: low, well-rounded ridge, stage 6: depressed bone level [84].

1.1.2. Bone reconstruction and regeneration

Clinicians are increasingly considering the use of dental implants for tooth replacement. Dental implants require quantitatively and qualitatively adequate bone condition to reach sufficient and predictable osseointegration. In some compromised prosthetic designs, due to insufficient bone volume, an undesired position must be used, or short implants must be placed to compensate for bone loss. This strategy often results in poor aesthetics and long-term treatment outcomes [18–20]. For this reason, numerous surgical approaches and bone

augmentation materials were developed as a tool for the reconstruction of atrophied alveolar bones and enhancement of bone regeneration.

1.1.3. Biomaterials

Autogenous bone grafts are the gold standard for augmentation procedures and have the potential to regenerate bone in this context three main mechanisms are important i.e. osteogenesis, osteoinduction, and osteoconduction. These grafts have not been shown to elicit an immune response.[21] Autogenous bone can be gained from different anatomic localization of the body; however, the process of harvesting autologous bone is reported to have numerous risks, such as the requirement for an additional surgical site and the risk of additional pain and complications at the donor site [22–24].

Bone substitute materials have been developed to avoid the disadvantages of autogenous bone. Various materials were introduced for clinical use in bone augmentation, reconstruction and regeneration, including autografts, allografts, alloplasts, and xenografts. Nevertheless, bone substitute materials do not exhibit properties of osteoinduction, and their capacity as osteoconductive materials varies. In addition to bone regeneration properties, the choice of the most suitable graft material have to be specific to the location of the graft site, the soft tissue quality, and its capacity to support implant osseointegration in future [11].

Various techniques have been developed for the augmentation and regeneration of atrophied bones based on the principles of GBR [18,25,26].

1.1.4. Guided bone regeneration (GBR) and guided tissue regeneration (GTR)

Extended atrophy in horizontal and/or vertical dimensions of the alveolar bone in future implantation area results in many clinical challanges. Successful implant osseointegration is the outcome of multiple processes including adequate bone regeneration, therefore bone augmentation is often unavoidable. The principle of GBR support the foreseeability of the augmentation process and promises long-term success and improve the implant integration within the regenerated bone region [11]. In this method, barrier membranes are used to promote bone regeneration by protecting against the undesirable ingrowth of fast migrating cellular populations from the overlying soft tissues to maintain space for the slow proliferating bone tissue and allow sufficient new bone formation (Figures 2 and 3) [27].
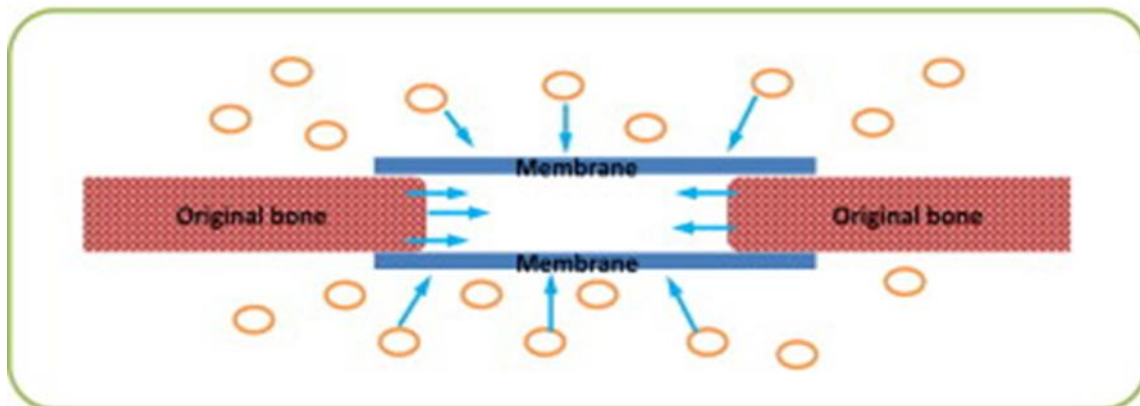
Figure 2: Concept of guided bone regeneration. Successful bone regeneration is based on the presence of two cellular components in the tissue, the slow migrating osteoblasts and the rapidly proliferating cells (fibroblasts and other soft connective tissue cells) [26.]

Requirements of the membrane include biocompatibility, material integration and mild inflammatory reaction without adverse reaction to achieve clinical success on the long term [28,29].

Furthermore, the membrane stability should serve as a barrier to exclude the ingrowth of fibrous tissue and protect the augmentation area from bacterial contamination [29,30]. Sufficient stiffness is also important to maintain space for bone regeneration [31]. Finally, the biomaterials must be clinically manageable in terms of enduring external forces such as mastication until blood clot has matured to support the membrane [32].
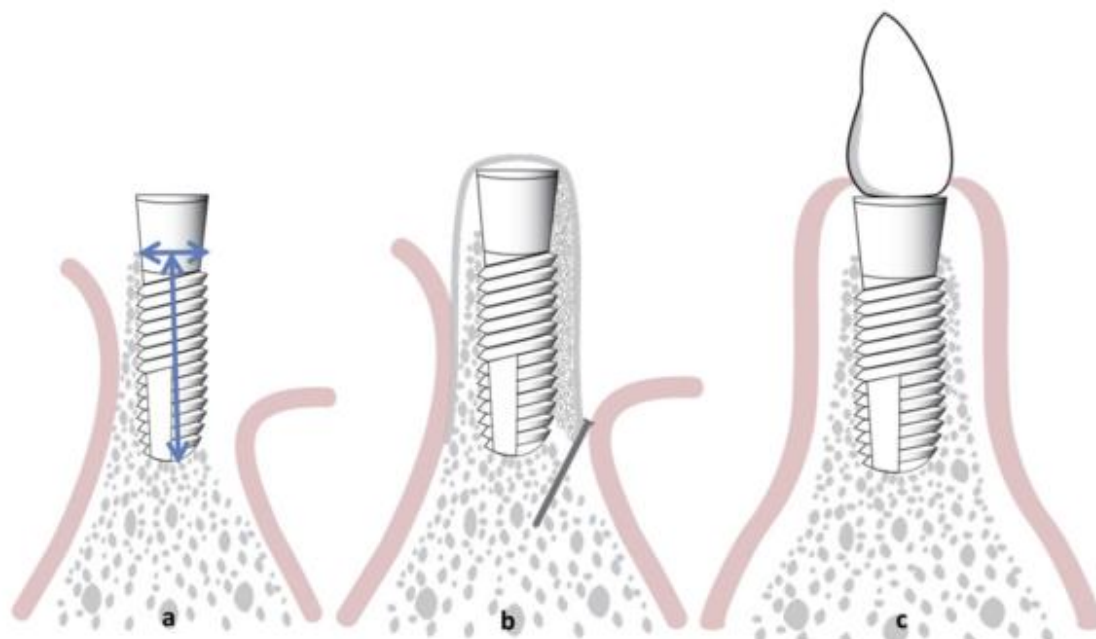
Figure 3: (a) An inadequate bone volume (height and width). (b) A barrier membrane and bone graft as bone substitute materials are placed to accelerate bone formation and protect against fast proliferating tissue ingrowth. (c) After new bone is formed, the final prosthesis is fabricated [26].

Further clinical application for memebranes is the soft tissue regeneration in sense of guided tissue regeneration (GTR) within the oral cavity [33,34] or in the extraoral region [35]. Alike GBR, GTR is surgical procedure that is performed to regenerate the soft tissue.[36] The strategy to isolate the bone or soft tissue defect with using biomaterials (either resorbable or non-resorbable) that should serve as a barrier to avoid rapid migrating epithelial cell invasion into the wound space. The membrane barrier provides a great chance for cementum, periodontal ligament, and bone cells to dominate the defect. In addition, they stabilize the blood clot and accelerate the differentiation of progenitor cell [36,37].

1.1.5. Membranes

GBR/GTR membranes are mainly classified into two classes, nonresorbable and resorbable membranes, based on their degradation potential.

Nonresorbable membranes, such as PTFE membranes, exhibit a high biocompatibility and hzdrophobicity. They provide a physical barrier and prevent the connective tissue to entry the bony defect. Therefore, a favorable correlation has been found between the level of bone regeneration and the maintained space for bone regeneration by PTFE-membranes [38].

Nonresorbable membranes have been reported to exert a greater effect on bone regeneration than resorbable membranes. This finding is explained by a persistent effect of the membrane on inhibiting soft tissue invasion as a physical barrier [39]. However, one of the most important disadvantages of nonresorbable membranes is the second surgical intervention that is needed to remove the membrane from the augmentation area after a predefined healing period. Additionally, the frequently observed high rate of membrane exposure resulting from wound dehiscence in accompanied by a risk of infection in the augmentation area [39].

Resorbable membranes have been developed to eliminate the need for a second surgical procedure [40]. These absorbable membranes are either based on collagen or noncollagen membranes.

Collagen-based membranes are derived from different species, such as porcine, equine and bovine.

Membranes of bovine origin are accompanied by a lot of concerns about the possibility of xenotransplantation of bovine spongiform encephalitis, although no such cases were reported in the literature [41]. However, animal-derived collagen-based membranes undergo strict purification, sterilization and processing procedures to manufacture membranes with a thickness of 0.5 mm to 1 mm for clinical use [36].

Clinical and histological analyses using with collagen based membranes resulted in initial tissue healing within a time frame of 5–7 days and membrane degradation after various time periods [42].

Membrane	Constitution	Tissue sources	Method of cross-linking	Resorption time
BioMend	Type I	Bovine (tendon)	Formaldehyde	6-8 weeks
BioMend Extend	Type I	Bovine (tendon)	Formaldehyde	18 weeks
Tissue Guide	Atelocollagen + Tendon	Bovine (tendon+dermis)	HMDIC	4-8 weeks
BioBar	Type I	Bovine (tendon)	N/A	24-32 weeks
Periogen	Type I and III	Bovine (dermis)	Gluteraldehyde	4-8 weeks
Cytoplast RTM	Type I	Bovine (tendon)	N/A	26-38 weeks
Symbios	Type I	Bovine (Achilles tendon)	N/A	26-38 weeks

Table 2: Available collagen membranes of bovine origin [15, 42].

1.1.6. Wound healing and tissue reactions.

After every surgical intervention, a wound healing process occurs to regenerate the tissue. Coordinated interactions between diverse biological and immunological systems take place in the wounded site to regenerate the damaged tissue, which is called physiological wound healing process. To improve the understanding of the physiological wound healing process, it can be divided into a series of four time-dependent phases:

1. Coagulation and hemostasis,

2. Inflammation,

3. Proliferation,

4. Wound remodeling [43].

Coagulation and hemostasis phases

Immediately after tissue damage, coagulation and hemostasis occur in the wounded site to prevent the loss of blood (exsanguination) by protecting the integrity of the vascular system [44]. Extrinsic and intrinsic pathways activate the coagulation cascade, which result in a platelet aggregation and clot formation in order that limit further blood loss. Moreover the blood clot serves as an interim framework for cellular migration in the phases following and the trapped platelets in the clot area are essential for haemostasis.

Inflammatory phase

This phase of wound healing aim to establish an immunological barrier against invading microorganisms which result in an infection [45]. The inflammatory phase is divided into two time-dependent phases, i.e. the early inflammatory phase and the late inflammatory phase.

Early inflammatory phase

The early inflammatory response occurs during the late phase of coagulation, 24 - 36 hours. Neutrophils are as first responder cells which attracted by chemoattractants and start to adhere to the endothelial cells or margination following by moving through the blood vessel wall or extravasation (diapedesis). After injury neutrophils infiltrate into the wounded site then destroy and remove foreign particles and damaged tissue especially bacteria contamination by releasing proteolytic enzymes and oxygen-derived free radical species [46].

Late inflammatory phase

In the late inflammatory phase, 48 - 72 hours, the originally blood monocytes are attracted to the wounded site by several of chemoattractive agents. Thereafter the blood monocytes undergo a phenotypic change to become tissue macrophages upon arrival into the wound [47]. Macrophages play the crucial role of the key regulatory cells for repair in the later inflammatory process. They serve as phagocytic cells and also related to the primary producer of growth factors responsible for the proliferation. Finally lymphocyte enter to the wound site, which are attracted about 72 hours after tissue damage by the action of interleukin-1 (IL-1), complement components and immunoglobulin G (IgG) breakdown products [43].

Proliferative phase

The proliferative phase begins on the third day after tissue damage and can be take more time to 14 days. Fibroblast is the characteristic for this phase by fibroblast migration and the deposition of newly synthesized extracellular matrix and formation of granulation tissue. Fibroblasts appear in the wound 2 - 4 days after tissue damage and the migration of endothelial cells take place following about 1 day afterwards. Once within the wound fibroblasts and myofibroblasts proliferate for the first 3 days and subsequently produce collagen and fibronectin.

These components help to form the new extracellular matrix, that supports further ingrowth of cells and is essential for the regeneration process. Furthermore fibroblasts are attracted to the wound by factors like PDGF & TGF-β thereafter tissue injury, in which its extracellular matrix consists of fibrous structural proteins (collagens and elastin).

Wound contraction take place begin approximately 7 days after injury. This process is mainly mediated by myofibroblasts, which align themselves parallel to the wounded surfaces then contract to wound edges closure together at a rate of 0.6-0.75mm/day, depends on the laxity of the skin. After accomplishing this task, they are eliminated by apoptosis [45].

Wound remodeling

The last stage of wound healing continues to form for several months up to 2 years so as to develop the normal epithelium and maturate the scar tissue. A balance between synthesis and degradation is essential, as type I collagen replaces by type III collagen. The type III collagen bundles are larger and oriented with principal lines of stress in tissue, these process results in a better organized wound. However, as the matured scare, it never reaches the level of unwounded tissue tensile strength. After completing this stage, the scars become grayish-pale and avascular, as an effect of decreasing vascularization over time [45].
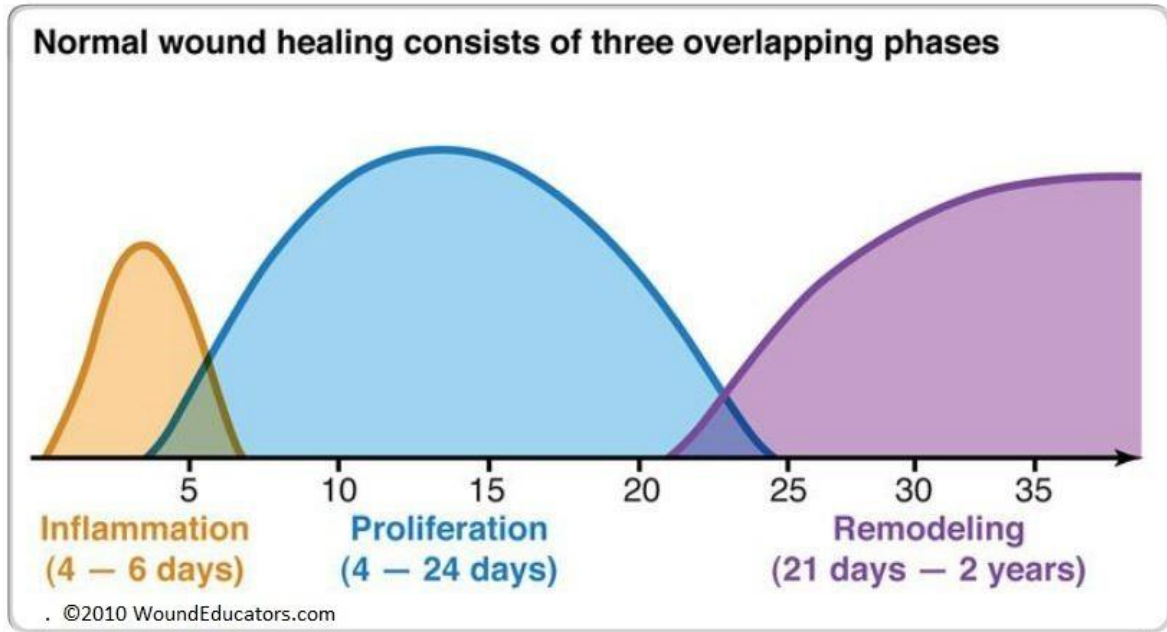
Figure4: Phases of wound healing [48].

1.2. Aim of the present study

After biomaterial implantation, a complex process of biomaterial-based regeneration takes place. This process is composed of the phases of wound healing and the biomaterial-induced cellular reaction. Numerous studies by our group have shown that the biomaterial-specific cellular reaction has major consequences for the regenerative capacity of the tissue. In this sense, the induced cellular reaction depends on the physicochemical properties of the biomaterial, i.e., thickness, porosity, cross-linking, origin and compartment from which it was harvested.

The present study aimed to assess the tissue response to the SYMBIOS® collagen membrane SR (Dentsply Implants, Germany), which is stated to be a slowly resorbable collagen type I membrane. An in vivo subcutaneous implantation model was used to analyze the cellular reaction towards this biomaterial over 30 days and obtain a better understanding of the mechanism of biomaterial-based tissue regeneration using this specific biomaterial derived from bovine Achilles

tendon. The cellular inflammatory pattern and vascularization level were analyzed using histological and immunohistological techniques and quantified by histomorphometry.

In addition, an ex vivo analysis using injectable platelet-rich fibrin (i-PRF), a blood concentrate system produced by the centrifugation of human peripheral blood that contains fibrin, leukocytes and platelets, was performed to elucidate the membrane permeability and interactions with human cells and plasma proteins.

2. Materials and methods

2.1. Biomaterial

SYMBIOS® Collagen Membrane SR

SYMBIOS® Collagen Membrane SR (SB, Dentsply implants, Germany) is a slowly resorbable membrane matrix composed of a highly purified type I collagen fibers gained from bovine Achilles tendon. The harvested collagen undergoes purification and processing with sodium hydroxide to inactivate pathogens such as bovine spongiform encephalopathy (BSE). The processing and purification methods meet European and international standards for animal tissue sourcing.

2.2. Study design

Study design

> In vivo
> (Implantation)

> Ex vivo
> (Liquid preparation)

Tissue processing

Sectioning & staining

Qualitative evaluation

Histomorphometric analysis

Statistical analysis
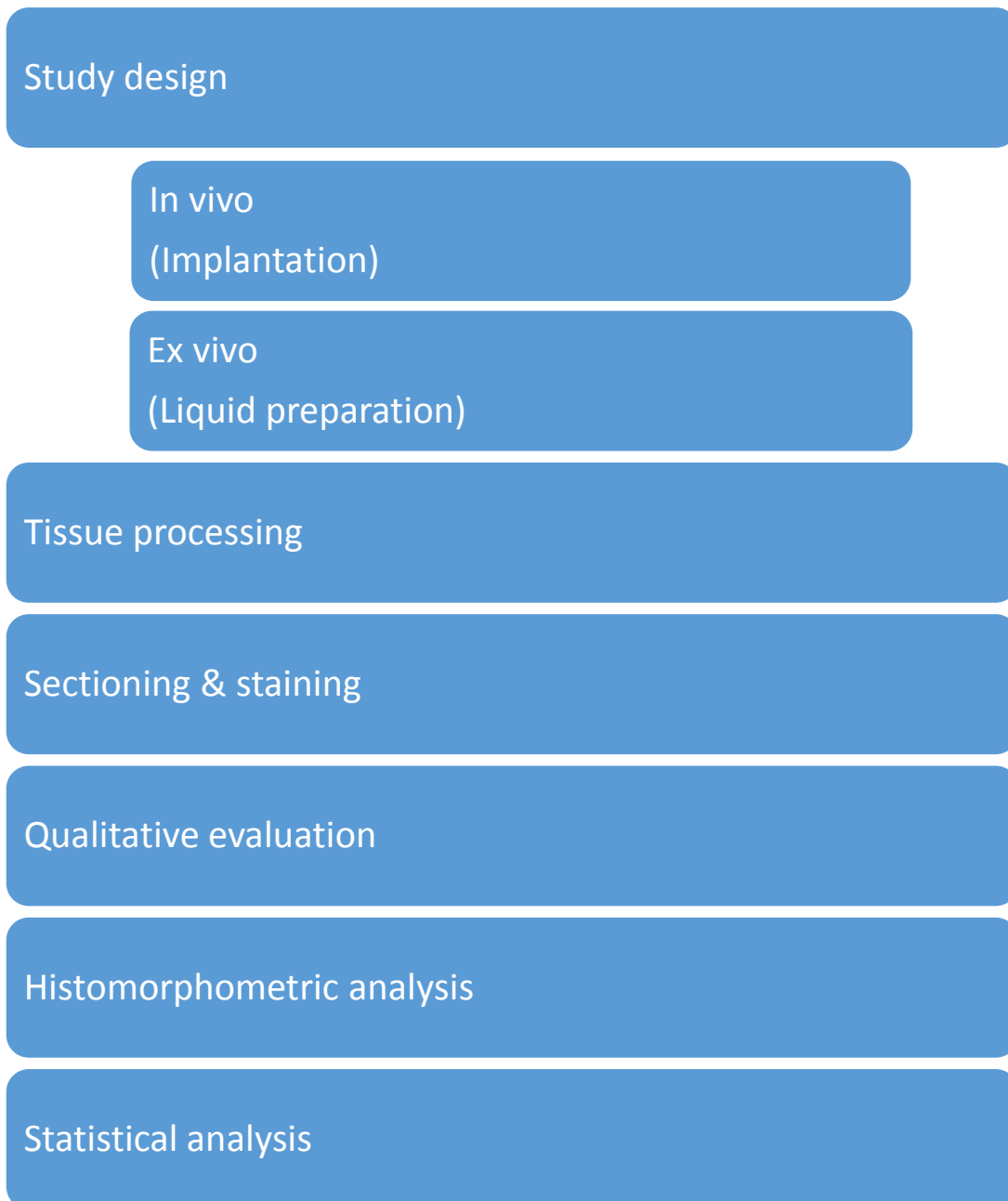
Diagram 1: Study design

2.3 Ex vivo evaluation of the biomaterial

The biomaterial structure and surface were evaluated ex vivo under dry conditions using a stereo-microscope (Zeiss, Deutschland), without further sample preparation.

2.3.1. Experimental design of the ex vivo study

The application of PRF in this study was performed in accordance with the principle of informed consent and approved by the responsible Ethics Commission of the state of Hessen, Germany (265/17). PRF is a blood concentrate derived from human venous blood through centrifugation without using anticoagulants [49]. An injectable formulation of PRF (i-PRF) was developed for practical clinical applications, which can be used alone or combined with biomaterials. Furthermore, PRF harbors a large number of platelets, leukocytes and plasma proteins distributed within the liquid fibrinogen matrix, and growth factors [49–51].

2.3.2. i-PRF preparation and application

In the ex vivo study, three healthy volunteers aged from 20 and 60 years donated blood. All volunteers provided written informed consent before participating in this study. The venous blood was collected and processed as previously described [52]. Clinically approved butterfly needles and 10 ml sterile plastic tubes (i-PRF tubes, PROCESS for PRF, Nice, France) were used. Blood samples from each donor were collected into two 10 ml tubes and immediately centrifuged using a preprogramed centrifuge (DUO™, PROCESS for PRF, France). Centrifugation was performed for 8 minutes at 600 rpm and 44 g, as fellowing the low speed centrifugation concept as previously [49, 51]. Upon completion of this process, a yellowish-orange upper phase (i-PRF) and the remaining reddish blood materials in the lower phase were observed in the tube. Then, the tubes were opened carefully to avoid homogenization of the material. The i-PRF was collected from the tubes using a 5 ml syringe (Injekt®, Germany)

with a needle (BD Microlance™ 3, Germany). Nine biomaterial samples (3 per donor) with a size of 10x10 mm were placed in a 24-well plate. Then, 1 ml of i-PRF was added to each biomaterial sample and incubated for 15 minutes until the i-PRF formed a clot. Thereafter, samples were fixed with 4% buffered formalin for 24 hours for further histological analysis.
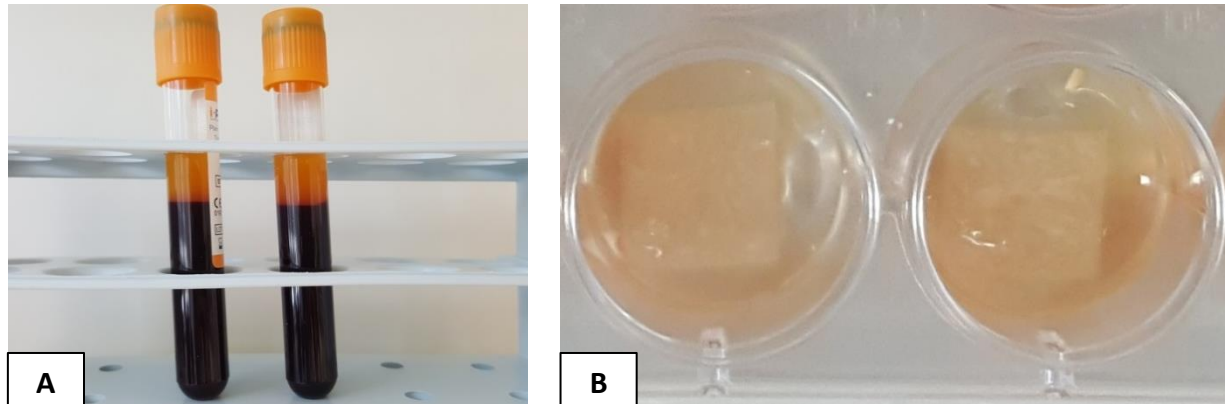
Figure 5: A) Injectable platelet-rich fibrin, B) Membranes + iPRF

2.4. Experimental design of the in vivo study

The present in vivo study used to elucidate the tissue reaction to collagen-based materials was performed after receiving approval from the Committee on the Use of Live Animals in Teaching and Research of the State of Darmstadt, Hessen Germany (FK/1023).

2.4.1. Experimental animal care

Thirty-two 6- to 8-week-old female Wistar rats were purchased from Charles River Laboratories (Sulzfeld, Germany) and allowed to recover and adapt to the conditions of the laboratory for one week prior to the surgical procedure in the Animal Welfare Officer and Central Facility (ZFE), Universitätsklinikum Frankfurt. There was performed following the ARRIVE guideline checklist for reporting

animal research. During the experiment period, the animals regular mouse pellets (Laboratory Rodent Chow, Altromin, Lage, Germany) and water was available ad libitum. An artificial 12 hours light-dark cycle was employed to imitate day and night rhythms.

2.4.2. Animal surgery

The animals were randomly distributed into 2 groups (n=16 animals per group). The following time points were evaluated in each group: 3, 10, 15 and 30 days post operation (n=4 animals per time point). Animals in the first group were implanted with a sterile collagen membrane (SYMBIOS® Collagen Membrane SR, Dentsply implants, Germany), whereas the second group received the sham operation (n=4 animals per time point) with no biomaterial implantation to ensure surgical quality. The surgical procedure was performed using standardized methods, as previously described.[53] Briefly, after an intraperitoneal injection of anesthesia, the operation area was shaved and desinfected. Next, an incision was prepared within the rostral portion and a subcutaneous pocket was prepared in the portion of the interscapular region. SB membranes of 10x10 mm in size were placed into the preformed subcutaneous pockets in the subscapular region under the muscle. After the incision and biomaterial implantation, the wound was subsequently stitched using a 6.0-prolene suture (Ethicon, New Jersey, USA). The surgical operations were performed respecting under strictly aseptic conditions. All animals survived the operation until the evaluated time points without any complications.

Figure 6: Pocket preparation in the subcutaneous implantation model

2.4.3. Explantation and fixation

At the evaluated time points, animals were sacrificed by an anesthesia overdose. The biomaterials, including the peri-implantation region in the first group and the sham-operated region of the second group, were explanted, and the ex vivo samples were process by a previously described method [52]. Briefly, the samples were fixed with 4% buffered formalin for 24 hours for further histological preparation.[28,52–54] After 24 hours, the each sample was divided into three segments prior to processing. Thereafter, the samples were transfered into embedding cassettes (Histosette, VWR, Germany). Paraffin embedding was performed after the specimens were dehydrated in a series of alcohol solutions, and the specimens were then transferred to xylene. This process was performed using a preprogramed tissue processor machine (Leica, Germany), according to the previously published method shown in Table 3 [52].

Reagent	Time (Minute)
4% Formalin	-
70% Ethanol	45
96% Ethanol	45
96% Ethanol	60
100% Ethanol	45
100% Ethanol	60
100% Ethanol	60
Xylol	45
Xylol	45
Xylol	45
Paraffin	45
Paraffin	120

Table 3: Tissue processor (dehydration and paraffin infiltration procedures)

2.5. Sectioning and histochemical staining

After sufficient cooling, the prepared, paraffin-embedded samples were cut to prepare serial sections of 3 to 4 μm thickness by means of a rotatory microtome (Rotationsmikrotom RM2255, Leica, Germany). After deparaffinization and rehydration, the in vivo and ex vivo samples were stained. The staining served as a method for identifying cells in the prepared tissue sections based on color reactions which were observed under a light microscope. Staining was performed as described in previous studies [28,52,55].

The first section was stained with hematoxylin and eosin (H&E), a standard histological stain used to visualize cell nuclei and other features.

The second section was stained with Heidenhain's azan trichrome to display various components of the connective tissue.

Masson's/Goldner's trichrome staining was used to distinguish collagen and muscle tissue under the microscope.

The fourth section was stained with tartrate-resistant acid phosphatase (TRAP) to examine TRAP activity in the cells, as previously described [52,55–57] The overview of various staining procedures used in different tissue sections is shown in Table 4, and the staining protocols are described afterwards.

	H&E	Masson/Goldner-Trichrome	Heidenhain's Azan Trichrome
Nuclei	Blue-purple	Dark blue to black	Bright red
Cytoplasm	Red	Red-brown	Purple-red
Collagen fiber	Red- orange	Light green	Blue
muscle	red	Pale blue	Orange-red
TRAP staining: intense light red detection of the enzyme Tatrat-resistant acid phosphatase (TRAP) in i.e. osteoclast-like cells and macrophages			

Table 4: Overview of the staining procedures used to assess various tissue components.

2.5.1. Hematoxylin and eosin (H&E)

The most commonly used stain is H&E, which is essential for visualizing an overview of the tissue structure, enabling differentiation of the structures being examined as normal, inflamed, degenerative or exhibiting pathological changes. The principle of H&E staining is that the basic, positively charged hematoxylin binds to basophilic substances, such as DNA/RNA, in the nucleus, whereas the negatively charged eosin dye stains the positively charged hydrogen ions in the cytoplasm [58].

The staining of the first section was performed manually according to the staining procedure book of the routine laboratory at FORM-Lab (Frankfurt

Orofacial Regenerative Medicine), the Research Laboratory of the Department for Oral and Maxillofacial Surgery, Goethe University, Germany using the protocol described below.

	Reagent	Time (Minute)
Deparafinization and rehydration	Xylol	5
	Xylol	5
	Xylol	5
	100% Ethanol	3
	100% Ethanol	3
	96% Ethanol	3
	70% Ethanol	3
	50% Ethanol	3
	Distilled water	3
Staining	Mayer's Hematoxylin	10
	Washing in running tap water	10
	Eosin Solution	5
	Washing in running tap water	Second
Dehydration	70% Isopropylalkohol	2
	96% Isopropylalkohol	2
	100% Isopropylalkohol	2
	100% Isopropylalkohol	2
	Xylol	3
	Xylol	3
	Xylol	3

Table 5: Protocol for Hematoxylin and Eosin (H&E) staining

Staining solution	Reagents and preparation
Hematoxylin solution	1 g Hematoxylin Monohydrate (VWR 1.15938.0100) in 1000 ml distilled water, dissolve hot until a slight color change to violet, then leave overnight. 50 g Potassium aluminium sulfate (VWR 1.01042.1000), 0.2g Sodium iodate ($NaIO_3$) (VWR 6526.0025), 50g Chloral hydrate ($C_2H_3Cl_3O_2$) (VWR 1,02425.1000), 1g Citric acid monohydrate ($C_6H_8O_7.H_2O$) stir overnight at room temperature. Bring the total volume up to 1000 mL. Filter and store in a dark bottle at room temperature. The Solution is protected from light at room temperature for 1 Year.
Eosin Solution	10 g Eosin water-soluble (CHROMA 1B 425) in 1000 ml distilled water heat with stirring until the substance is completely dissolved. Filter before use and acidify with acetic acid. (4 Drops Acetic acid pro 100 ml Eosin solution) (VWR 1.00063.1011) The Solution is protected from light at room temperature for 6 months.

Table 6: Protocol for the preparation of hematoxylin and eosin solutions

2.5.2. Masson's/Goldner's trichrome staining

This staining method is used for differentiated visualization of connective tissue. Three different stains are used:

a. Weigert's iron hematoxylin for nuclei

b. Mixture of acid dyes (Biebrich scarlet-acid fuchsin) for cytoplasm

c. Light green for collagen. The method is a standard staining procedure for bone; thus, the use of Masson's/Goldner's trichrome also provides information about bone remodeling [59,60]. The protocol for Masson's/Goldner's trichrome staining and the composition and preparation of the required reagents are presented in Tables 7 and 8.

	Reagent	Time (Minute)
Deparafinization	Xylol	5
	Xylol	5
	Xylol	5
	100% Ethanol	3
	100% Ethanol	3
	96% Ethanol	3
	70% Ethanol	3
	50% Ethanol	3
	Distilled water	3
Staining	Weigert's hematoxylin	5
	Washing in running tap water	10
	Distilled water	Wash up
	0.5% Phosphotungstic acid	15-30 second
	Scarlet-acid fuchsin-Azophloxin solution	10
	1% Acetic acid	Wash up

	1% Acetic acid	Wash up
	1% Acetic acid	Wash up
	Phosphotungstic acid/Orange G	10
	1% Acetic acid	Wash up
	1% Acetic acid	Wash up
	1% Acetic acid	Wash up
	Light green solution 0,2%	5
	1% Acetic acid	Wash up
	1% Acetic acid	Wash up
	1% Acetic acid	Wash up
	100% Isopropanol	3
	100% Isopropanol	3
	100% Isopropanol	3
	Xylol	3
	Xylol	3

Table 7: Protocol for Masson's/Goldner's trichrome staining

staining solution	Reagents and preparation
Weigert's hematoxylin	Solution A – CHROMA, 2E 032 Solution B – CHROMA, 2E 052 Equal parts. The Solution is protected at room temperature for 1 month.
Scarlet-acid fuchsin solution (Masson solution)	0,2 g Xylidine ponceau (Chroma 1B207) 0,1 g Acid fuchsin (VWR 223K18010831) in 300 ml Distilled water. Boil briefly, Cool down 0,6 ml Acetic acid (VWR 1.00063.1011) Filter, The Solution is protected from light at room temperature for 12 months

Azophloxin solution	0,5 g Azophloxine (Chroma 1B103) 100 ml Distilled water. 0,2 ml Acetic acid (VWR 1.00063.1011) The Solution is protected from light at room temperature for 12 months.
Scarlet-acid fuchsin- Azophloxin solution	10 ml Masson solution (Scarlet-acid fuchsin solution) 2 ml Azophloxine solution 88 ml 0,2 % Acetic acid (2 ml Acetic acid in 1000 ml distilled water) The Solution is protected at room temperature for 1 month
1% Acetic acid	10 ml Acetic acid (VWR 1.00063.10011) in 1000 ml distilled water. The Solution is protected at room temperature for 6 months
Phosphotungstic acid/Orange G	3g Phosphotungstic acid hydrate (VWR 1.00582.0100) 2 g Orange G (VWR 15925 – 25 g) 100 ml distilled water The Solution is protected from light at room temperature for 12 months
Light green solution	0,2 g Light Green SF (Chroma 1B211) 100 ml Distilled water. 0,2 ml Acetic acid (VWR 1.00063.1011) The Solution is protected from light at room temperature for 12 months

Table 8: Protocol for preparing the Masson's/Goldner's trichrome solution

2.5.3. Heidenhain's azan trichrome staining

Heidenhain's azan trichrome staining was developed based on the traditional Mallory method and uses azocarmine instead of acid fuchsin. It is useful for distinguishing cells from extracellular materials [58]. The protocol for Heidenhain's azan trichrome staining and the composition and preparation of the required reagents are shown in Tables 9 and 10.

	Reagent	Time (Minute)
Deparafinization	Xylol	5
	Xylol	5
	Xylol	5
	100% Ethanol	3
	100% Ethanol	3
	96% Ethanol	3
	70% Ethanol	3
	50% Ethanol	3
	Distilled water	3
Staining	Kernechtrot Solution	30
	Washing in running tap water	Wash up
	Washing in running tap water	Wash up
	Distilled water	Rinse in running water 1 minute
	5% Phosphotungstic	10
	Distilled water	Wash up
	Azan solution	5
	Distilled water	Wash up
	100% Isopropanol	Until the finest connective tissue fibers are well defined
	100% Isopropanol	2
	100% Isopropanol	2
	Xylol	3
	Xylol	3
	Xylol	3

Table 9: Protocol for Heidenhain's azan trichrome staining

Staining solution	Reagents and preparation
Kernechtrot Solution	0.2g Kernechtrot (VW 15939) In 100ml 5% Aluminium sulfate solution 5 minute Boil Filter before use The Solution is protected from light at room temperature for 12 months
Aluminium sulfate solution	5g Aluminium sulfatev(VWR 1102) In 100ml distilled water
5% Phosphotungstic acid	25g Phosphotungstic acid hydrate (VWR 582) in 500ml distilled water The Solution is protected at room temperature for 3 months
Azan solution	Stock solution : 0,5g Anilin blue (VWR 1275) 2g Orange G (VWR 15925) in 100ml distilled water Boil briefly 8ml Acetic acid (VWR 1.00063.1011) Filter before use The Solution is protected from light at room temperature for 12 months Working solution : 1 Part Anilin blue Orange + 3 parts Distilled water The Solution is protected at room temperature for 1 month

Table 10: Protocol for the preparation of Heidenhain's azan trichrome staining solution.

2.5.4. Tartrate-Resistant Acid Phosphatase (TRAP)

The enzyme TRAP is expressed in osteoclasts, multinuclear giant cells, macrophages, dendritic cells and a number of other cell types. The TRAP staining protocol and the composition and preparation of the required reagents are shown in Tables 11 and 12.

	Reagent	Time (Minute)
Deparafinization	Xylol	5
	Xylol	5
	Xylol	5
	100% Ethanol	3
	100% Ethanol	3
	96% Ethanol	3
	70% Ethanol	3
	50% Ethanol	3
	Distilled water	3
Staining	TRAP solution	150
	Washing in running tap water	Wash up
	Washing in running tap water	Wash up
	Distilled water	Wash up
	Mayer's hematoxilin	5
	Washing in running tap water	10
	Distilled water	Wash up
	Aquatex	cover

Table 11: Protocol for tartrate-resistant acid phosphatase (TRAP) staining.

Staining solution	Reagents and preparation
Tris-Malein-Puffer:	13,14 g TRIS (Fa. Roth 48552) 11,60 g Maleic acid (VWR 8.00380.0500) 31,20 ml 1 N NaOH (VWR 109137.1000) in 2000 ml Distilled water adjust to pH 5.8 The Solution is protected at 2 - 8 °C temperature for 6 months
Naphthol AS-BI phosphate (SIGMA NN 250)	Storage at 2 - 8 °C temperature for 12 months
Diazonium solution	1 Drop. 4 % Pararosaniline solution 4 Drops. 4 % Sodium nitrite solution Mixing and allow to react for at least 5 minutes The Solution is in use in 3 hours at 37 °C
Pararosaniline solution	1 g Pararosaniline (VWR 7601) 25 ml 2 N-HCl (VWR 1.09063.1000) Heat at 50 ° C for 1 hour on the magnetic stirrer until the solution appears brownish, filter, cap and keep in dark at 4 ° C. The Solution is protected at 2 - 8 °C temperature for 1 year.
Sodium nitrite solution	0,2 g Sodium nitrite (VWR 1.06549.0100) in 5 ml distilled water. The Solution is protected at room temperature for 1 week.
Dimethyl sulfoxide (VWR 8.02912.1000)	
L-(+)-Tartaric acid (VWR 1.00804.0250)	Weighed in 75 mg portions The Solution is protected at 2 - 8 °C temperature for 1 year.
Hematoxylin solution	2,5 g Hämatoxylin (VWR 104302.0100) in 2500 ml distilled water dissolve in hot condition until color change into a slightly violet. then cool down overnight. then add and dissolve with stirring : 125 g Aluminium potassium sulfate dodecahydrate (VWR101042.100) 0,5 g Sodium iodate (VWR 6525.0025) 125 g Chloral hydrate (VWR 102425.1000) 2,5 g Citric acid hydrate (VWR 244.1000)

| | Incubation for 1 week, filter before use |
| | The Solution is protected at room temperature for 1 year. |

Table 12: Protocol for the preparation of tartrate-resistant acid phosphatase solutions.

2.5.5. Immunohistochemical staining

Two more sections of the in vivo samples were used for immunohistochemical staining to determine the blood vessel density and number of biomaterial-associated macrophages with antirabbit vWF and antimouse CD-68 antibodies, respectively [52–54] Immunohistochemical staining was performed after deparaffinization using a Lab Vision™ Autostainer 360-2D (Thermo Fisher Scientific, Germany), quenching the endogenous peroxidase activity using 4% H_2O_2 in methanol and blocking using avidin and biotin blocking solutions (Avidin/Biotin Blocking Kit, Vector Laboratories, USA). The first antibody, anti-CD-68 (MCA341GA; 1:400; 30 minutes), was applied to visualize macrophages, and the anti-vWF antibody (ab6994; 1:400; 2 hours) was applied to visualize vascular endothelial cells. Thereafter, the goat antirabbit IgG-B secondary antibody (sc-2040; 1:200, Santa Cruz Biotechnology, USA) was applied. Thereafter, the avidin-biotin-peroxidase complex (ABC, Thermo Fisher Scientific, Germany) and the histostain-plus IHC Kit including AEC (Thermo Fisher Scientific, Germany) were applied for 30 minutes and 20 minutes, respectively. The staining protocols are described in table 13. As negative controls, immunohistochemical staining was performed on 2 control sections in the absence of the primary antibody, whereas the positive control was performed according to the manufacturer's instructions (anti-CD-68, rat lymph node and anti-vWF, human tongue). For visualization by light microscopy, the sections used for immunohistochemistry were counterstained with Mayer's hematoxylin.

Procedure	Time (Minute)
Check all the necessary solutions or reagents	
Prepare and prewarm pretreatment solution and deparaffin and rehydration	
Wash in TBS	2
Wash in TBS	2
Incubate the slides in 0.3% H2O2	10
Wash the slides in TBS	2
Wash the slides in TBS	2
Incubate in Bioblock1	10
Wash in TBS	2
Wash in TBS	2
Incubate in Bioblock2	10
prepare the primary antibody before the end of blocking	
wash in TBS	2
wash in TBS	2
incubate in primary antibody (for von Willebrand Faktor, 1:50 diluted in antibody dilution solution) for 30 min	30
wash in TBS	2
wash in TBS	2
incubate in secondary antibody (Rabbit-B 1:200, diluted in antibody dilution) for 30min (immediately prepare the ABC solution)	30
wash in TBS	2
wash in TBS	2
incubate in ABC	30
wash in TBS	2
wash in TBS	2
develop color with AEC at Room temperature	3
rinse in running dest water	5

counter staining	20
embedding in water mounting solution	

Table 13: Immunohistochemistry protocol for von Willebrand Faktor

2.6. Qualitative histological analysis

The qualitative histopathological evaluation was performed as described in previous publications [52,54] Briefly, cross-sections stained by various protocols were evaluated under a light microscope (Eclipse 80i, Nikon, Tokyo, Japan), and representative photomicrographs were performed using a digital camera (Nikon DS-Fi1, Nikon, Tokyo, Japan). The processed samples were examined histologically to analyze the cellular interactions within the peri-implant tissue and the membrane in addition to the cellular response that took place inside the implanted material, i.e. the recruitment of inflammatory cells and vascularization induced by the biomaterials along with biomaterial degradation. A further aim of the histological analysis was to examine the interaction of the biomaterial with i-PRF ex vivo.

2.7. Histomorphometric analysis

The quantitative histomorphometric analysis of stained slides was performed with a light microscope (ECLIPSE 80i; Nikon, Tokyo, Japan) equipped with a motorized scanning stage (ProScan III, Prior, Rockland, MA, USA) and a Nikon DS-Fi1 digital camera (Nikon, Tokyo, Japan) connected to a PC running NIS Elements software (Nikon). Using established and previously published methods [28,52,55], images of the total implantation beds (total scans) were obtained as a single large image of the sample, including the collagen membrane and the peri-implant tissue; this image automatically comprised 100-130 individual micrographs. The images were merged and then total scan images were evaluated at a magnification of x100 and a resolution of 2500x1200 pixels.

2.7.1. Membrane thickness

Previously reported histomorphometric methods were used to obtain information about the stability of the volume of the biomaterial at the implantation site [52,55]. Total scans of the H&E-stained slides were used to measure the mean membrane thickness at each time point. At least 15 distinct locations along the length of the biomaterial were manually measured in each animal using the "length measurement" function in the "Annotation and Measurements" feature of the NIS Elements software (Figure 7). The mean value of these measurements per sample was measured as the absolute membrane thickness in μm. The data gathered from later time points were calculated as percentages, and the thickness recorded on day 3 was set to 100% to avoid artifacts due to the histological preparation.
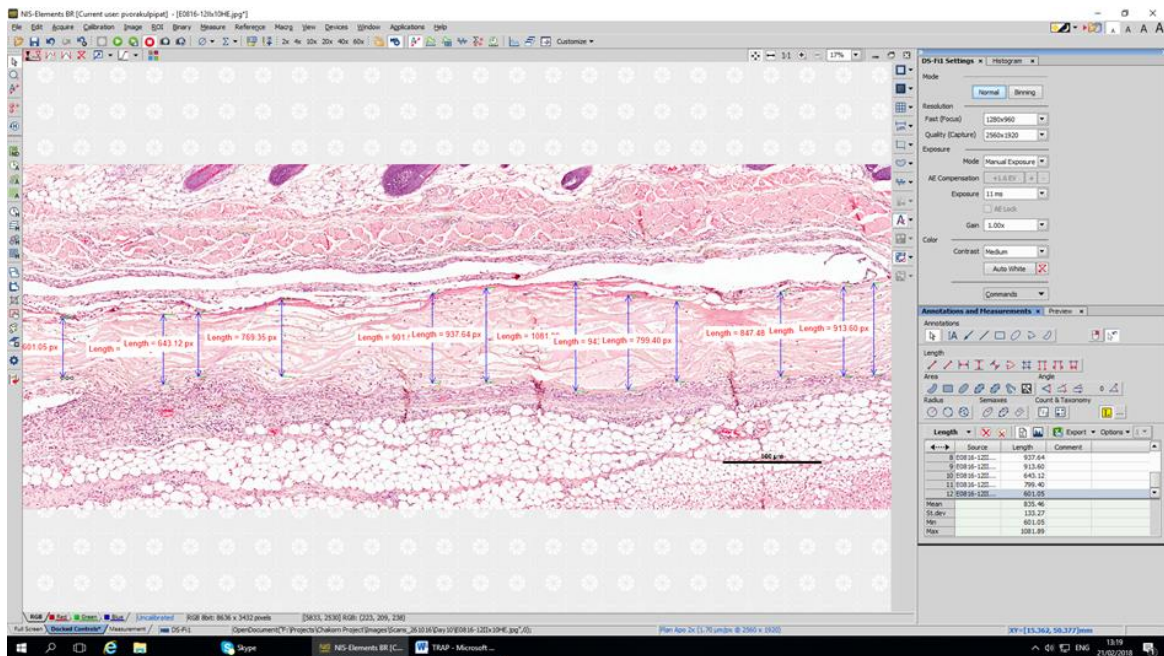

Figure 7: Membrane thickness, histomorphometrical analysis using NIS Elements software

2.7.2. Numbers of multinucleated giant cells (MNGCs) and CD-68-positive mononuclear cells

The numbers of MNGCs and TRAP- positive MNGCs and CD-68-positive monocytes were counted manually to analyze the material induced cellular reaction in the implantation region. Digital images of the stained samples were captured as previously described [52]. The numbers of MNGCs and their subtypes (TRAP-positive and -negative giant cells) and CD-68-positive mononuclear cells were counted independently in total scans of the TRAP and CD-68 staining from each animal using the ''count'' tool in NIS Elements (Figure 8). The total numbers of the cell types were calculated with respect to the total implant area on the slides (cell number/mm²) at each time point. The histomorphometrically evaluated data was analyzed statistically to understand the cellular reaction induced by the implanted biomaterial SB in comparison to the physiological wound healing over the observation time of the study.
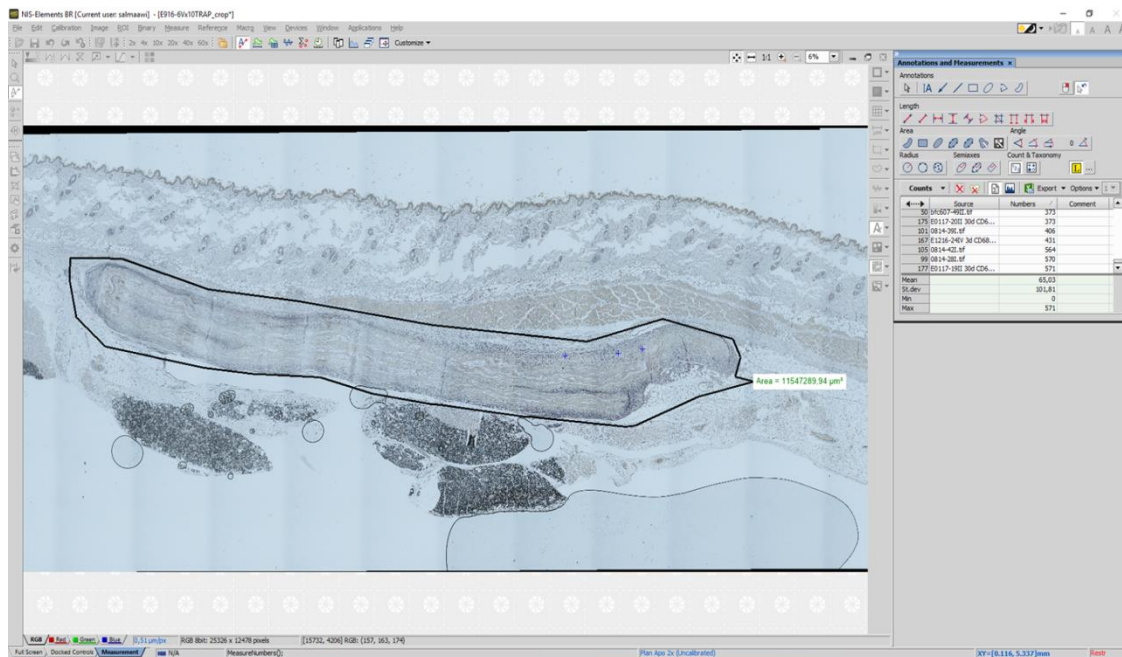

Figure 8: Numbers of multinucleated giant cells.

2.7.3. Measurements of membrane vascularization

The vWF-stained slides were used to evaluate two different vascularization parameters according to previously published methods [52,55]. Initially, digital images of the vWF-stained slides were captured. Then, the area of the implantation bed of the biomaterial (in mm²) was measured using the "Annotation and Measurements" feature of the NIS Elements software (Figure 9). Subsequently, the vessels within the implantation beds were marked. Thus, the total number of vessels was calculated relative to the total area (in vessels/mm²) and as a percentage of vessel area (the fraction of the total implant area as a %).
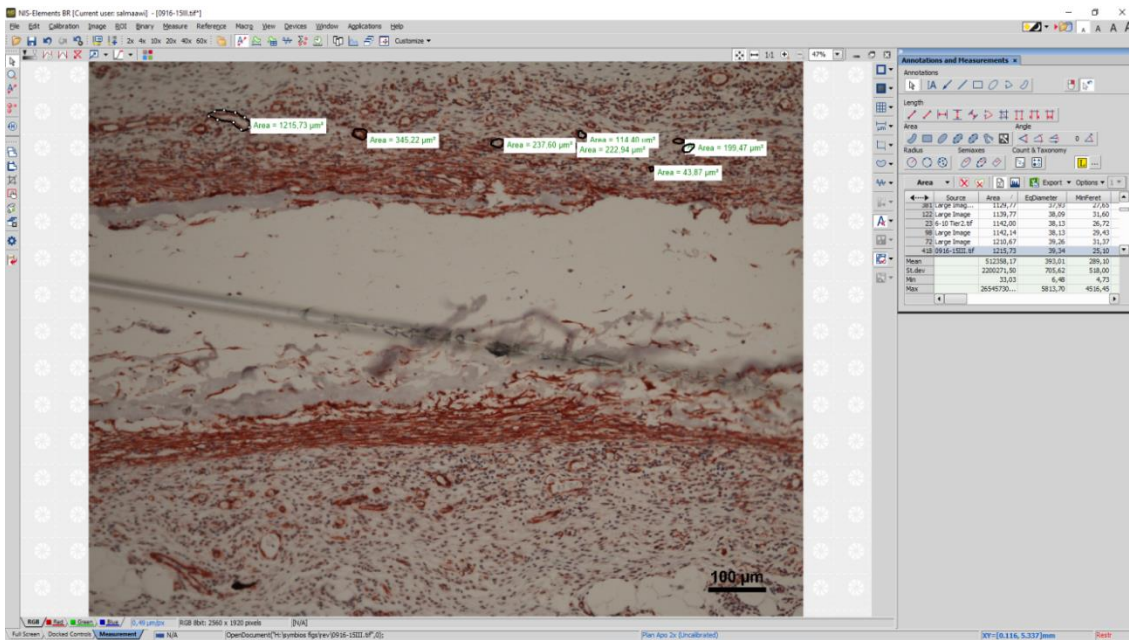

Figure 9: Histomorphometrical measurement of the vascularization by determining the vessels´areas

2.8. Statistical analysis

Histomorphometricaly gained values were further analyzed statistically using two methods one way analysis of variance (ANOVA) for membrane thickness and MNGCs number. Two-way analysis of variance (ANOVA) was performed for vascularization and CD68 positive cells. Statistical significance was defined as p-values */• p<0.05; **/•• p<0.01; ***/••• p<0.001 and ****/•••• p<0.0001, respectively, using GraphPad Prism software version 6.0C (GraphPad Software Inc., La Jolla, CA, USA). The results are presented as means±standard deviations calculated using GraphPad Prism 6 software version 6.0C, which was also to produce graphical images and perform statistical analyses.

3. Results

3.1. Ex vivo analysis of the membrane structure

The microscopic structural of the SB collagen membrane was observed under dry conditions at low magnification. The SB membrane exhibited a cord-like surface on both sides, as shown in Figure 10A and B. At a higher magnification, the membrane displayed a porous structure (Figure 10C and D), while a single-layer thin membrane composed of single fibrils was visible in the cross-section, as shown in Figure 10E.
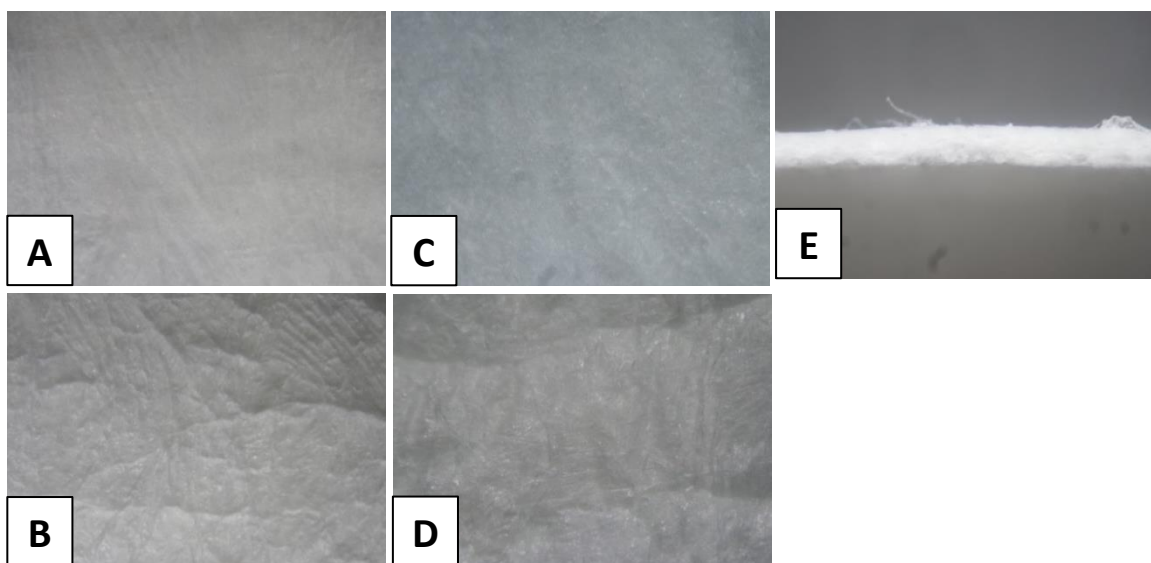

Figure10: Microscopic characteristics of the structure of the SB collagen membranes. The images in A, B, C and D show the structure of the SB membrane surface at different magnifications. The images shown in E displays cross-sections of the analyzed material. (Magnifications: 10A and B x8; 10C-E x32)

3.2. Ex vivo evaluation of the membrane-i-PRF interaction

The histological analysis of the native collagen membrane SB stained with H&E revealed a loose structure with detectable pores (Figure 11A). Fifteen minutes after i-PRF application, cells accumulated on the SB collagen membrane surface and leukocytes and platelets infiltrated the membrane central region. However, the formation of an adherent clot formation was not detected on either surface of the SB membrane (Figure 11).
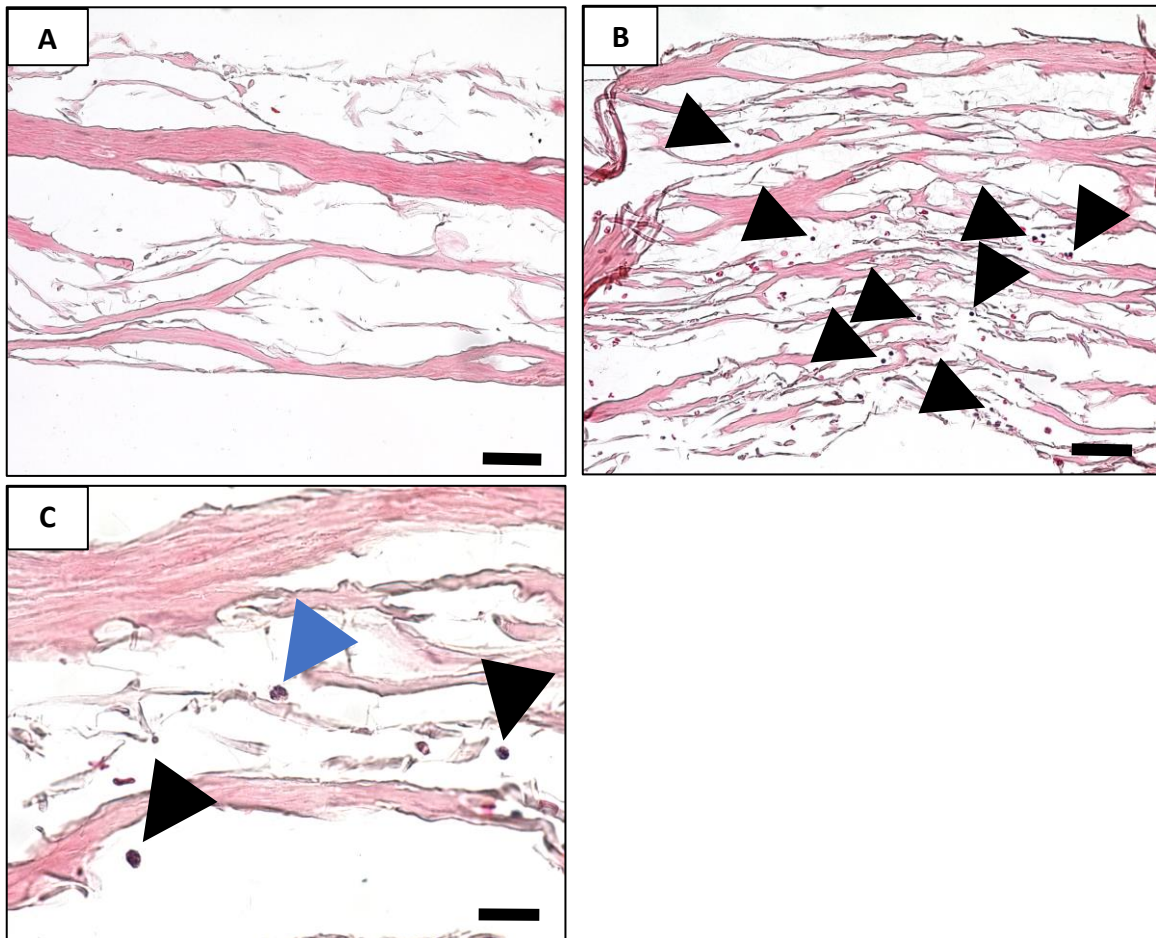

Figure 11: Ex vivo interaction between liquid platelet-rich fibrin and the SB collagen membrane. A: Image from the control group showing the membrane-specific porous structure (H&E staining; x10 magnification; scale bar=100 µm). B: Total penetration of leukocytes and platelets into the SB central region (H&E staining; x100 magnification; scale bar=100 µm). C: High-magnification microscope image showing the infiltration of

leukocytes and platelets throughout the central region of the membrane: leukocytes (blue arrow) and platelets (black arrow) (H&E staining; x600 magnification; scale bar=20 μm).

This figure was published [61].

3.3. In vivo histological and histomorphometric analyses

Throughout the study, all animals survived the operation and biomaterial implantation without any macroscopically observable disorders. Wound healing was uneventful in the test group and the control group. No signs of infection, necrosis or atypical animal eating and sleeping behaviors were observed during the evaluation period.

3.3.1. Qualitative analysis of the cellular reaction over time

The biomaterial was visible within the implantation region at all time points. At 3 days after implantation, no signs of membrane degradation were observed, and the membrane maintained its native structure. Mononuclear cells were observed on both peri-implant interfaces (Figure 12A). The central region of the SB membrane generally did not exhibit evidence of cell infiltration, as shown in Figure 12B.
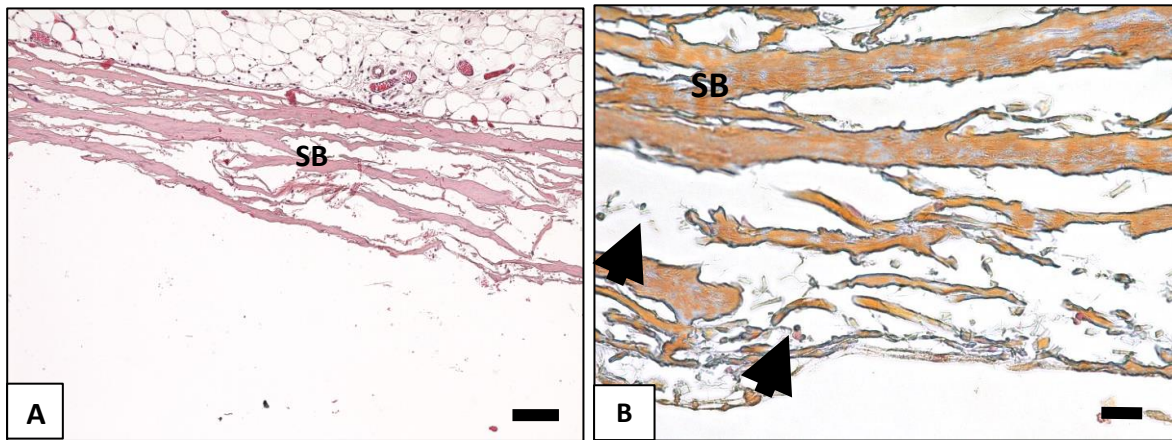
Figure 12: The cellular reaction after 3 days. A: The central region of the biomaterial was generally free of cells (H&E staining; x100 magnification; scale bar=100 µm). B: The presence of mononuclear cells on the surface of the membrane (azan staining; x400 magnification; scale bar=20 µm).

This figure was published [61].

On day 10 after implantation, the membrane margin was still markedly visible. The mononuclear cells that were first observed at day 3 had migrated and increased in number on both sides of the membrane. Moreover, mononuclear cells started penetrating inwards along the membrane and began to produce their own matrix within the SB collagen matrix (Figure 13A). Immunohistologically marked CD-68 positive mononuclear cells were present as macrophages within the peri-implantation tissue. (Figure 13B). A small number of MNGCs was detectable; these cells were mainly localized on the membrane surface and proximal region of the biomaterial. However, most of these cells were TRAP-negative (data not shown). Moreover, microvessels were detected in near to the biomaterial (Figure 13C).
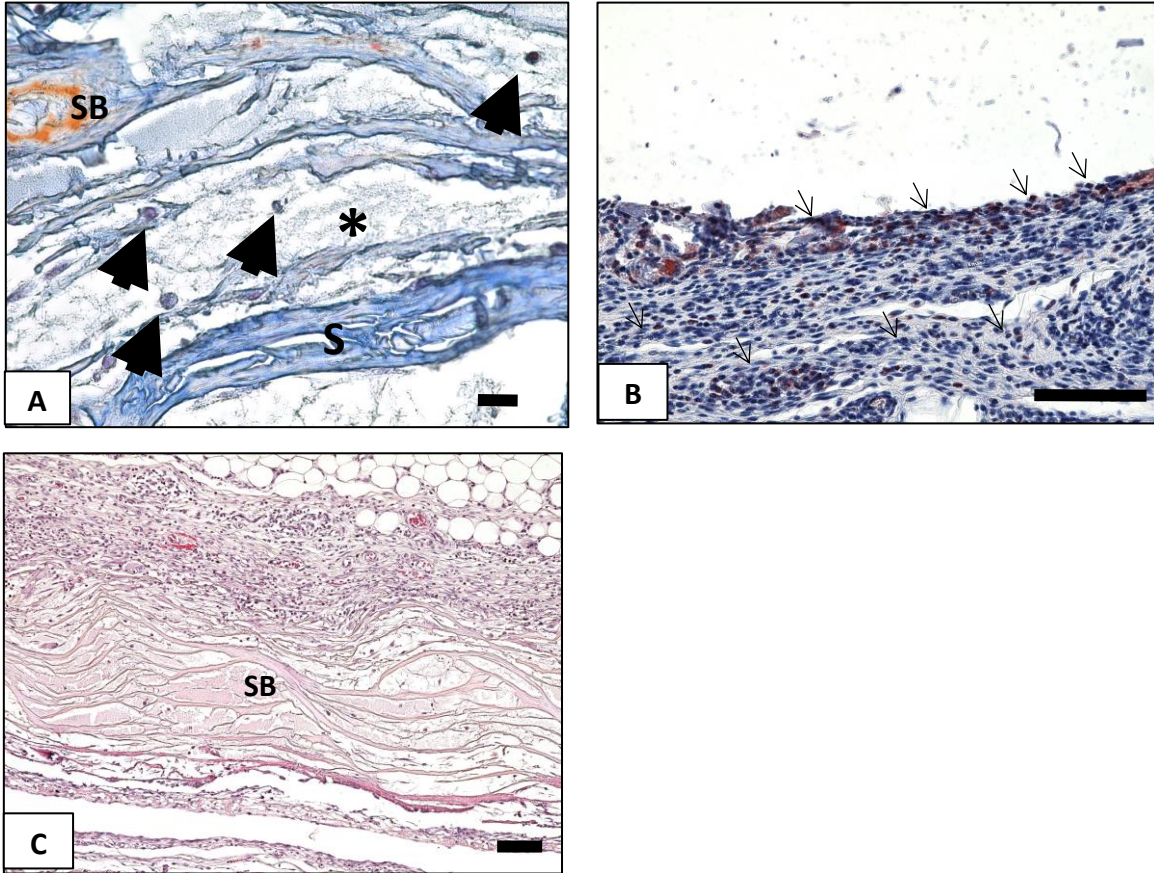
Figure 13: The cellular reaction after 10 days. A: Mononuclear cells started invading the membrane and were observed within the pores of the membrane (azan staining; x400 magnification; scale bar=20 μm). B: CD-68-positive macrophages accumulated on the biomaterial surface, most of which were TRAP-negative (CD-68 immunohistochemical staining; x200 magnification; scale bar=100 μm). C: Microvessels were detected in proximity to the biomaterial (H&E staining; x100 magnification; scale bar=100 μm).

This figure was published [61].

On day 15 after implantation, no evidence of membrane breakdown was detected. The mononuclear cells infiltrated throughout membrane and reached the central region of the membrane body (Figure 14A). The number of CD-68-positive macrophages, which were located in proximity to the biomaterial, was reduced compared to the number observed on day 10 (Figure 14B). Unlike, the number of

MNGCs was significantly increased, and these cells were generally TRAP-negative (Figure 14C). A richly vascularized connective tissue was readily observed in the peri-implantation area compared with the previous time point. Nevertheless, the central region of the membrane body remained avascular (Figure 14D). New connective tissue was generated within the membrane matrix, as depicted in Figure 14E.
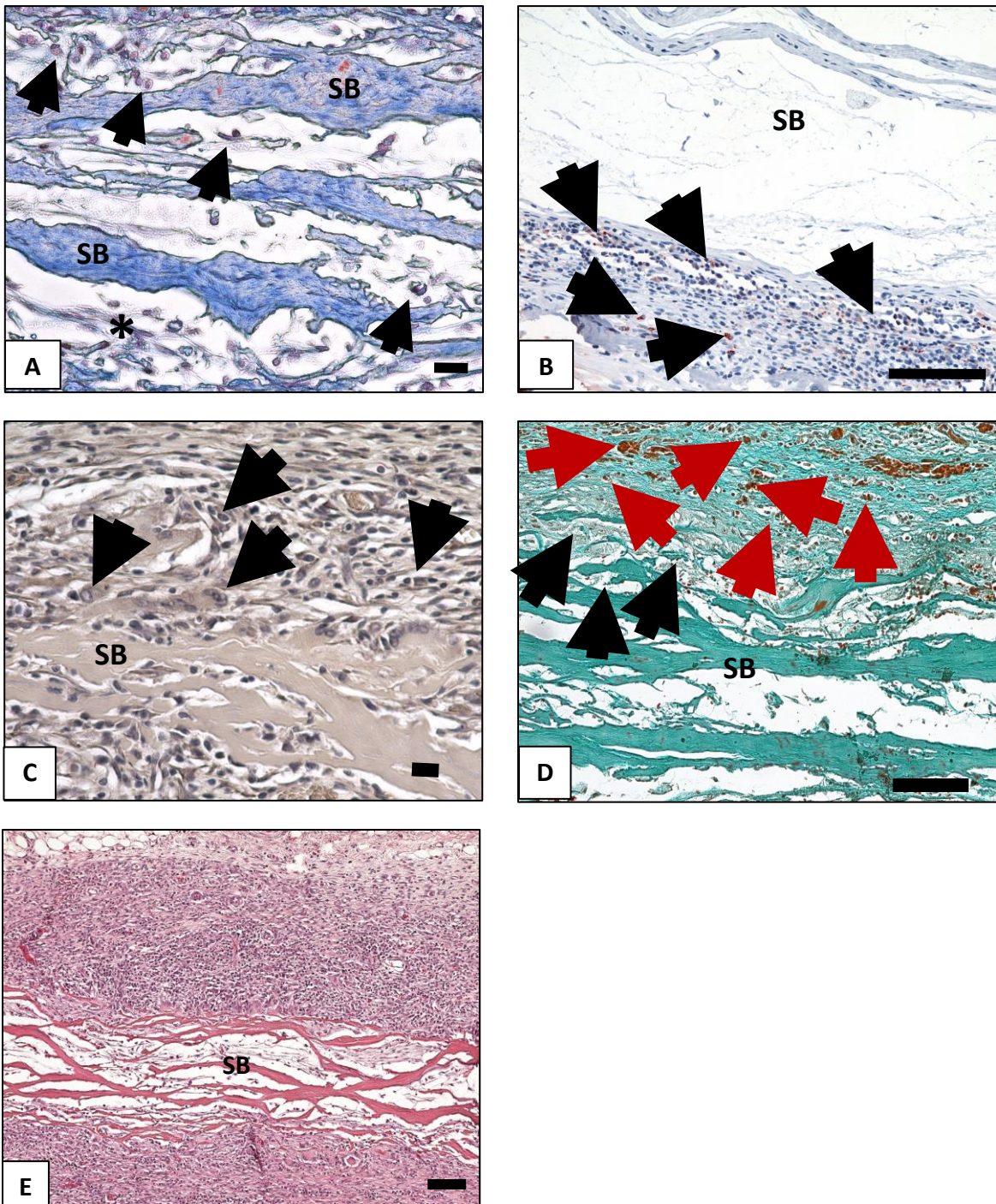
Figure 14: The cellular reaction after 15 days. A: More mononuclear cells invaded the membrane and reached the its central region, and the membrane interfibrillar area contained connective tissue (azan staining; x400 magnification; scale bar=20 µm). B:

Fewer CD-68-positive macrophages were observed in proximity to the biomaterial (CD-68 immunohistochemical staining; x200 magnification; scale bar=100 μm). C and D: The implantation bed showed greater vascularization than at the previous time point. However, no vessels were found within the central region of the membrane (C: TRAP-negative MNGCs (black arrow) TRAP staining; x400 magnification; scale bar=20 μm, D: MNGCs (black arrow) and adjacent vessel (red arrow) in Masson's/Goldner's trichrome-stained sections; x200 magnification; scale bar=100 μm). E: The implantation bed showed greater vascularization than at the previous time point. However, no vessels were observed within the central region of the membrane (H&E staining; x100 magnification; scale bar=100 μm).

This figure was published [61].

At day 30 postimplantation, the biomaterial was obviously detectable within the implantation region as a stable structure, and the integrity of the SB membrane was maintained. At this time point the membrane did not show any signs of degradation. The host mononuclear cells were allowed to penetrate and distribute throughout membrane, but the biomaterial maintained its native structure (Figure 15A). Biomaterial-adherent CD-68-positive macrophages were observed in the peri-implantation region near the implanted membrane interface (Figure 15B). The number of MNGCs did not display a drastic change. MNGCs were located adjacent to the membrane surface but were not able to penetrate into biomaterial central region. Furthermore, the MNGCs did not express TRAP (Figure 15C). A well-vascularized connective tissue wall was readily observed in the region surrounding the membrane at this time point (Figure 15D), while additional newly formed connective tissue was observed within the membrane matrix (Figure 15E).

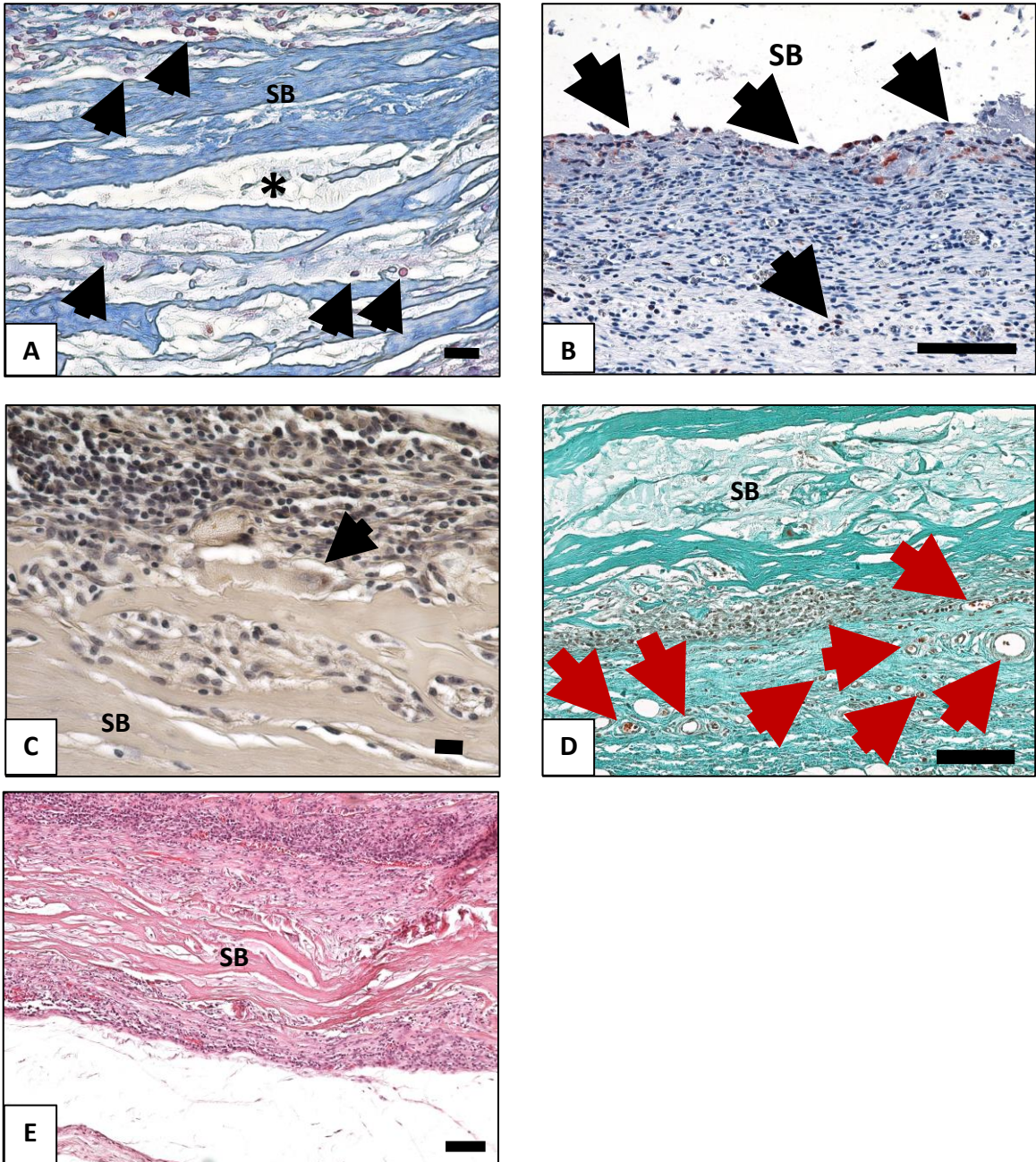Figure 15: The cellular reaction after 30 days. A: The membrane was embedded in the cell- and vessel-rich host connective tissue and allowed the infiltration of mononuclear cells and connective tissue into its central region without any degradation (azan staining; x400 magnification; scale bar=20 µm). B: Some CD-68-positive macrophages were observed in close proximity to the biomaterial (CD-68 immunohistochemical staining; x200

magnification; scale bar=100 µm). C and D: The implantation area exhibited well-vascularized new connective tissue, while the biomaterial retained its native structure and included the newly formed connective tissue (C: TRAP-negative MNGCs (black arrow) TRAP staining; x400 magnification; scale bar=20 µm, D: adjacent vessels (red arrows), Masson's/Goldner's trichrome staining; x200 magnification; scale bar=100 µm). E: The implantation area contained well-vascularized new connective tissue, while the biomaterial retained its native structure and included the newly formed connective tissue (H&E staining; x100 magnification; scale bar=100 µm).

This figure was published [61].

Animals in the control group, which underwent a sham operation, did not exhibit signs of macroscopic pathological conditions, i.e., tissue necrosis, hemorrhage, wound infection or atypical inflammation, and no signs of wound dehiscence were observed at any time points in the present study (data not shown). MNGCs were not detected at any time point. Only mononuclear cells were detected, and a large number of macrophages was observed on day 3. Then, the number of macrophages showed a significant decrease until day 30. Some vessels were observed on day 3 and showed a slight increase until day 30 (data not shown).

3.3.2. Quantitative histomorphometric analysis

3.3.2.1. Evaluation of the membrane thickness over time

The mean SB membrane thickness was measured in the total scanned micrographs using histomorphometry. The mean thickness of the biomaterial measured 3 days after implantation was considered the baseline (233.5±29.4 µm). The peak membrane thickness (366.4±104.8 µm) was observed on day 10. The increase in the membrane thickness was statistically significant (**p<0.001) compared to day 3. At 15 days postimplantation, the membrane thickness

(366.4±104.8 µm) tended to decrease compared to day 10; however, the difference was not statistically significant. Moreover, a similar thickness was observed over the course of implantation after 30 days (325.7±51.3 µm). The differences in thickness between days 10, 15 and 30 compared to day 3 were statistically significant at **p<0.01, *p<0.05 and *p<0.05, respectively. The differences in thickness for days 10, 15 and 30 were not statistically significant (Diagram 2).
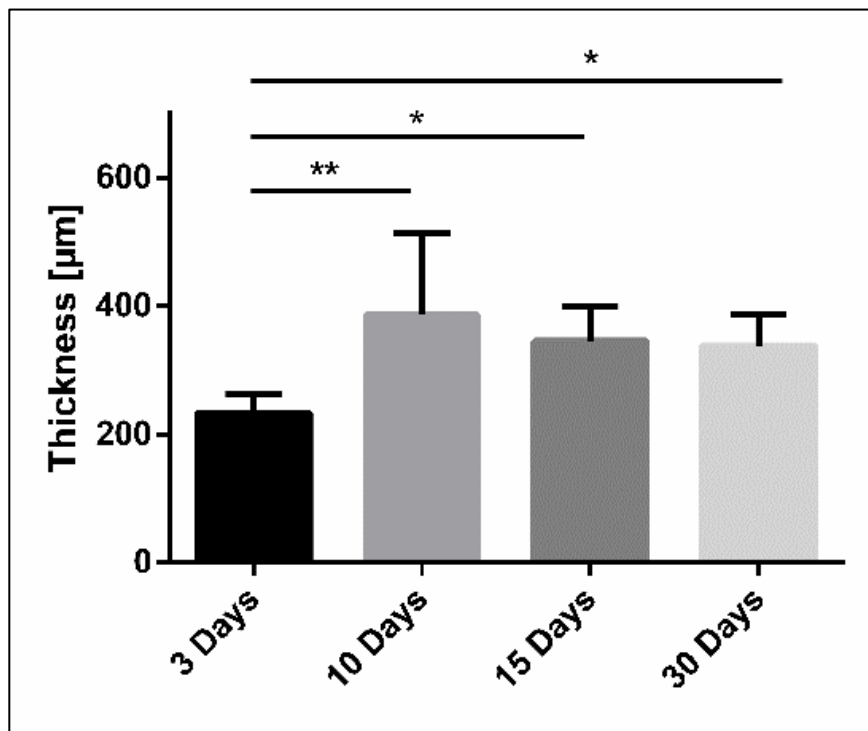

Diagram 2: Evaluation of the membrane thickness over time

Statistical significance was defined as p-values */• p<0.05; **/•• p<0.01;

/••• p<0.001 and */•••• p<0.0001

This diagram was published [61]

Consistent with the mean membrane thickness, the analysis of the percent thickness displayed a similar pattern. The thickness measured on day 3 was considered the baseline and was set to 100%. The thickness of the biomaterial increased on day 10 (149.2±13.5%). Fifteen days after surgery, the percent membrane thickness showed a slight reduction (134.5±12.1%) and then maintained the thickness until 30 days (139.9±8.2%). The differences in thicknesses between days 10, 15 and 30 were statistically significant compared to the value measured on day 3 at ****$p < 0.0001$, **$p < 0.01$ and ***$p < 0.001$, respectively. The differences for measurements recorded on days 10, 15 and 30 were not significant (Diagrams 2 and 3).
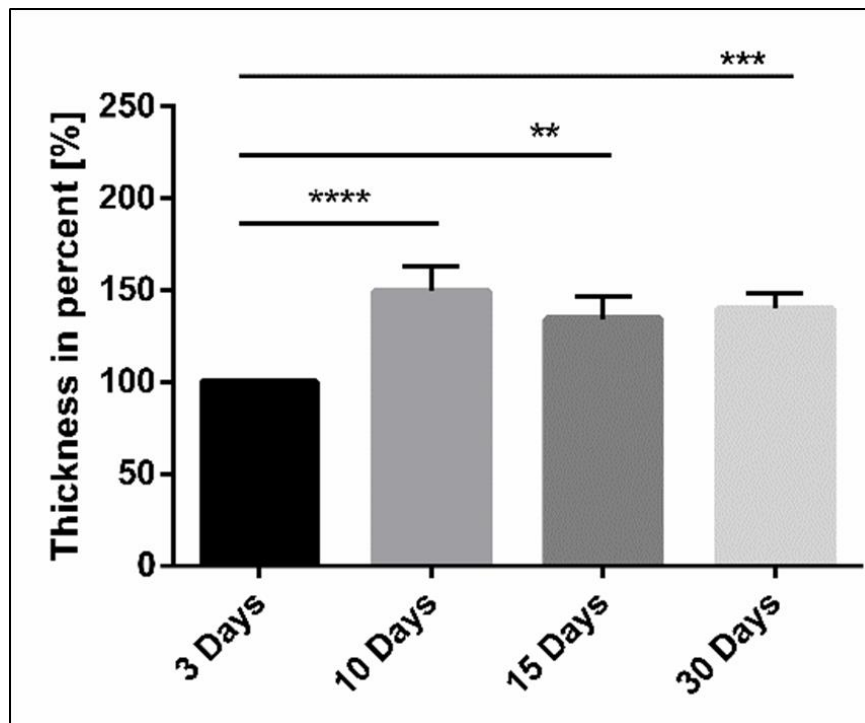

Diagram 3: Evaluation of the membrane thickness over time as a percentage

Statistical significance was defined as p-values */• $p < 0.05$; **/•• $p < 0.01$;

/••• $p < 0.001$ and */•••• $p < 0.0001$

This diagram was published [61]

3.3.2.2. Evaluation of the number of CD-68 positive cells (macrophages)

The macrophage density was evaluated by performing histomorphometric measurements of the CD-68-positive cells. The number of CD-68-positive cells drastically increased from 3 days (33.7 ± 12.5 cells/mm^2) to 10 days after implantation, and the peak cell density was observed on day 10 (185.9 ± 8.5 cells/mm²), a difference that was statistically significant at ****$p<0.0001$ compared to day 3.

At 15 days postimplantation, the cell number (118.9 ± 8.5 cells/mm²) was decreased compared to day 10, and the difference was statistically significant (***$p<0.001$). On day 30, the macrophage number reached a steady-state value (109.8 ± 14.4 cells/mm²), as the difference was not significant compared to day 15. The differences in cell density between days 10, 15 and 30 in comparison to day 3 were highly statistically significant at ****$p<0.0001$, ****$p<0.0001$ and ****$p<0.0001$, respectively.

Conversely, a greater number of CD-68-positive cells was observed in the control group than in the test group on day 3 following the surgical intervention (105.9 ± 16.3 cells/mm²), and the differences between the number of macrophages observed on day 3 and all other time points were statistically significant (****$p<0.0001$).

From day 3 to day 10, the number of macrophages in the control group decreased rapidly (19.6 ± 3.7 cells/mm²). A similar number of cells was observed on day 15 (12.5 ± 4.2 cells/mm²) and day 30 (8.9 ± 2.9 cells/mm²) as on day 10. The different numbers of macrophages observed between control and test group at each time point were highly statistically significant (••••$p<0.0001$) (Diagram 4).
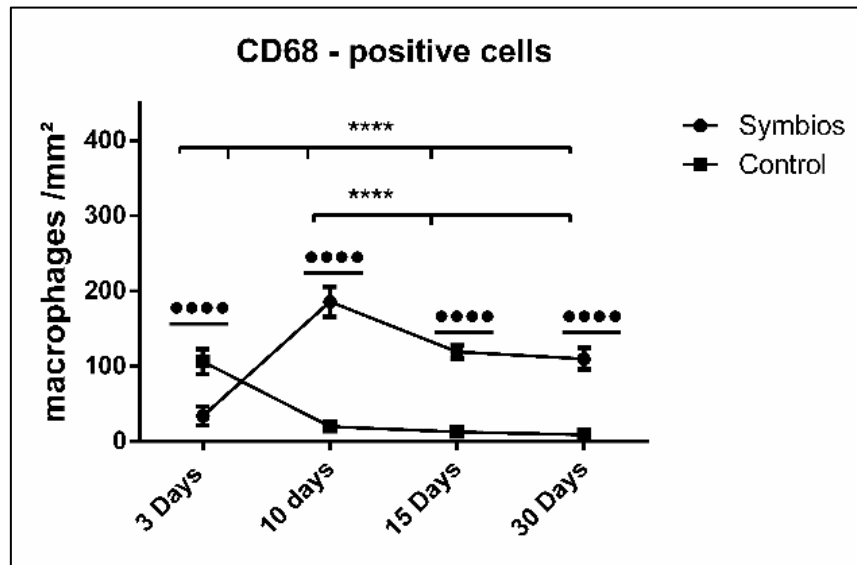
Diagram 4: Evaluation of the number of CD-68-positive cell (macrophage)

Statistical significance was defined as p-values */• p<0.05; **/•• p<0.01;

/••• p<0.001 and */•••• p<0.0001

This diagram was published [61].

3.3.2.3. Evaluation of the multinucleated giant cells number over time

The number of MNGCs was determined histomorphometrically per quadrate millimeter. After 3 days, no MNGCs were visible in the implantation area of the membrane. The number of MNGCs increased significantly on day 10 (4.6±1.3 MNGCs/mm², *p<0.05). Furthermore, the greatest increase in the number of MNGCs was observed on day 15 (9.3±2.1 MNGCs/mm²), and a statistically significant difference was observed in comparison to day 10 (*p<0.05). Then, the total number of MNGCs exhibited a slight decrease on day 30 (7.2±2.7 MNGCs/mm²); however, the difference was not significant compared to day 15. A significantly lower number of cells was observed on days 15 and 30 (****p<0.0001 and ***p<0.001, respectively) in comparison to day 3. Membrane-adherent TRAP-positive MNGCs were generally not detected; therefore, analysis was not

performed (Diagram 5). MNGCs were not detected in the control group at any time point during the study.
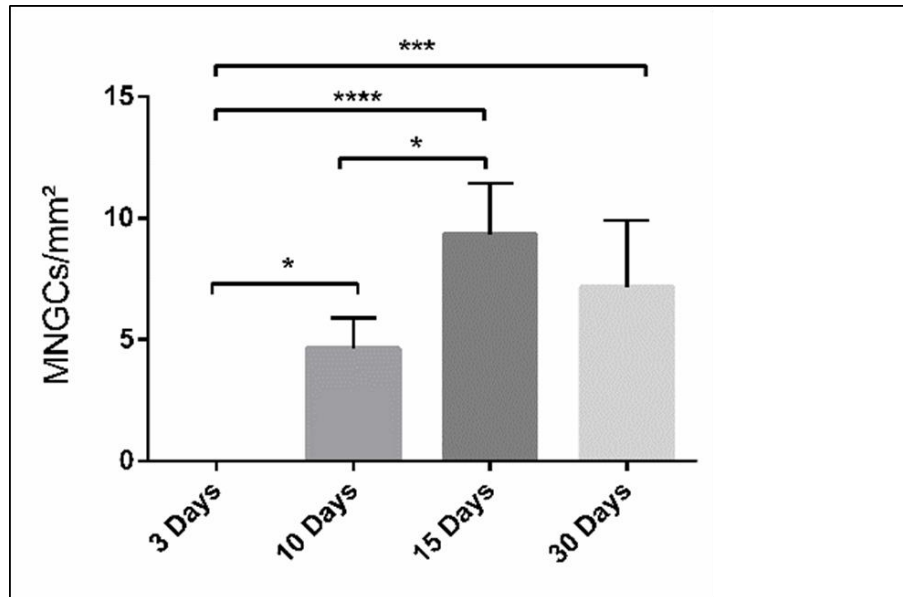
Diagram 5: Evaluation of the numbers of multinucleated giant cells over time

Statistical significance was defined as p-values */• p<0.05; **/•• p<0.01;

/••• p<0.001 and */•••• p<0.0001

This diagram was published [61]

3.3.2.4. Evaluation of the vascularization pattern

According to the histomorphometric measurements of the vessel density, vessels did not grow into the membrane over time, whereas mild vascularization was observed in the implant beds of the biomaterial on day 3 (6.4±2.8 vessels/mm²). On day 10, the peri-implantation area in the test group showed rapidly increasing vascularization compared to day 3 (33.7±8.4 vessels/mm²), and the difference was statistically significant (**p<0.01). Thereafter, the vessel density was steady (day 15: 35.4±13.4 vessels/mm²) and slightly increased on day 30 (39.4±8.8 vessels/mm²). However, the difference was not significant compared to

day 15. Moreover, significantly less vascularization was observed on day 3 than on days 10, 15 and 30 (**p<0.01 and ***p<0.001, respectively).

In contrast, the control group showed a mild vascularization on day 3 (5.3±2.7 vessels/mm²), which was comparable to the SB-implanted group. Then, the vessel density exhibited a gradually increasing trend over the observation time of the study: at day 10 (5.9±2.2 vessels/mm²), day 15 (6.3±3.8 vessels/mm²) and day 30 (10.2±2.1 vessels/mm²). The different numbers of the vascularization pattern observed between control and test group at each time point were highly statistically significant (••••p<0.0001) (Diagram 6).

Diagram 6: Evaluation of the vascularization pattern

Statistical significance was defined as p-values */• p<0.05; **/•• p<0.01;

/••• p<0.001 and */•••• p<0.0001

This diagram was published [61]

The analysis of the percentage of vascularization in the implantation bed compared to day 3 (0.2±0.07%) showed a similar pattern, with a substantial increase on day 10 (1.6±0.06%). The difference was statistically significant

(***p<0.001). A comparable vascularization rate was observed on day 15 (1.3±0.6%) compared to the values recorded on day 10. In addition, a similar value was also measured for the percent vascularization on day 30 (1.7±0.3%). Compared to the later study time points, a significantly lower percentage of vascularization was observed on day 3 was than on day 10 (***p<0.001), day 15 (**p<0.01) and day 30 (****p<0.0001) (Diagram 7).

Similar values for the percentage of vascularization were obtained from the sham-operation group. On the other hand, significant intra-individual differences were observed compared to the values of the control group recorded at later time points in the study: day 10 (****p<0.0001), day 15 (**p<0.01) and day 30 (**p<0.01). As on day 10, the evaluation of the vascularization pattern as a percentage observed between control and test group at each time point were statistically significant: day 10 (••••p<0.0001), day 15 (••p<0.01),, day 30 (••p<0.01) (Diagram 7).
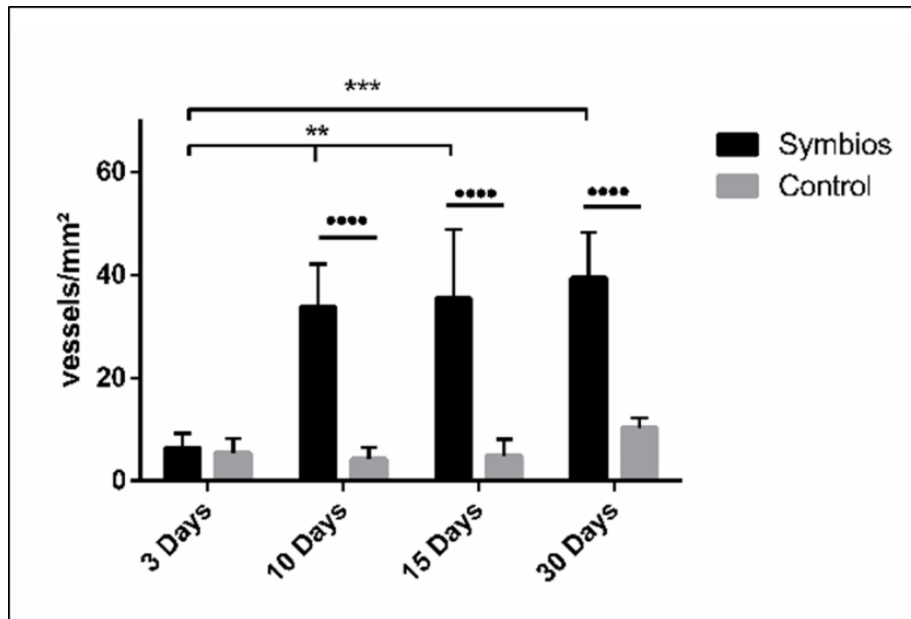

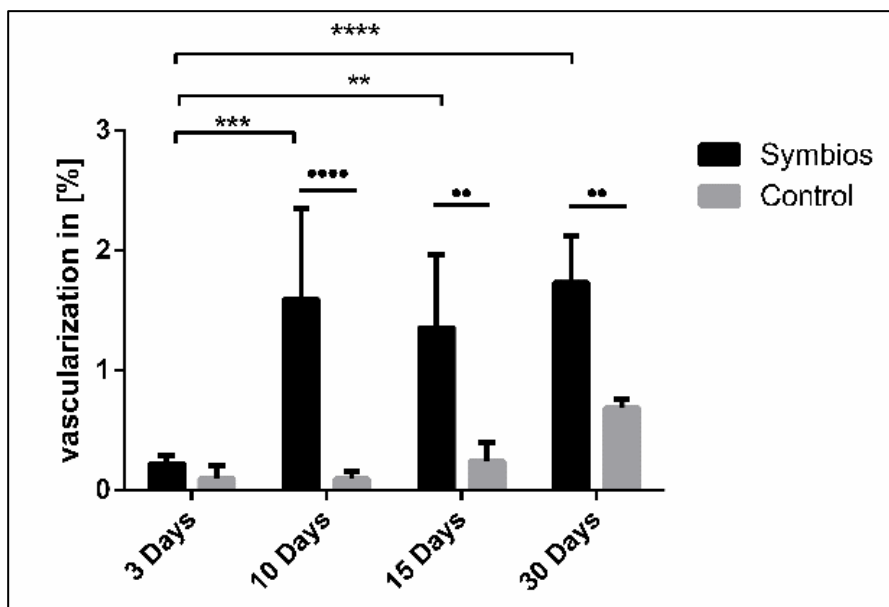Diagram 7: Evaluation of the vascularization pattern as a percentage

Statistical significance was defined as p-values */• p<0.05; **/•• p<0.01;

/••• p<0.001 and */•••• p<0.0001

This diagram was published [61]

4. Discussion

Currently, many biomaterials are used to regenerate bone and soft tissues, particularly in modern dentistry, which seeks to restore physiological form, function and aesthetics for patients who are missing teeth. A defined amount of bone is required for implant placement and integration to optimize tooth restoration and improve the patient's quality of life [56]. Moreover, periodontal treatments performed after the presentation of infra-bony defects are repaired by the placement of the periodontal apparatus, but new supporting tissue does not form. A particular concern for many patients is increasing gingival recession, which causes cosmetic problems and tooth sensitivity. One advancement to overcome some of these limitations is GTR, which is widely used and has healed periodontal tissue by promoting the formation of new attachment tissue [62].

This concept is also employed in tumor resection and defect reconstruction of intraorally located benign or malignant tumors, particularly in patients suffering from head and neck cancer, who, cause by their decreased life expectancy, must be rehabilitated to improve their already diminished quality of life. The utilization of GTR with a collagen membrane results in minimum flap mobilization and improves the functions of mastication and phonetics, while improving aesthetics [35].

Based on GTR principles within the host tissue, biomaterials should exhibit biocompatibility to allow host tissue integration without inducing a foreign body reaction, proper degradation, and stable integrity and volume of the implanted tissue region for an appropriate time period to improve tissue regeneration.[27,28,53] In the last decade, collagen-based materials have been introduced as favorable candidates for GTR applications due to their promising properties, such as their notable angiogenic potential [63,64] and delayed material degradation [65].

However, various collagen-based materials with different specific characteristics have been used in GTR/GBR. The use of the membrane purification method, materials of animal origin (porcine [28,53–55], bovine [66,67] and equine [68]) different sources for harvesting the material (pericardium [55], dermis [54],

tendon [52]) and the manufacturing and processing procedures influence the native structure. Different biomaterials induce different cellular reactions, depending on their specific physicochemical properties.

A recently published study evaluated a non-cross-linked collagen material derived from the porcine peritoneum combined with porcine skin using an in vivo subcutaneous implantation model in CD-1 mice. According to the histological findings, the material induced a tissue reaction associated only with mononuclear cells, such as macrophages, and no signs of MNGCs or premature breakdown were detectable during the observation period of 60 days. Moreover, transmembrane vascularization was not detected. These outcomes led the authors to conclude that collagen-based membranes for GBR applications are permeable to nutrients through diffusion processes and do not necessarily need membranous vascularization for good integration into the host tissue [15].

A subsequent study evaluated the tissue response to a noncross-linked collagen I-III-based matrix derived from the porcine peritoneum using the same animal model. The histological analysis showed that the collagen matrix attracted only mononuclear cells but did not undergo transmembrane vascularization. These findings were additionally translated to the clinic by performing a histological analysis of the membrane after application in recession coverage via GTR [28].

In contrast, two xenogeneic collagen membranes of porcine origin harvested from different compartments, i.e., the porcine pericardium and dermis, were investigated using the same in vivo model. Different types of tissue reaction were observed, as a significant increase in the number of MNGCs was observed over the study period of 30 days. The presence of MNGCs within the two noncross-linked, collagen-based biomaterials led to the premature loss of their native structure and disingration.[54,55] In this context, the cellular reaction to the different membranes was primarily related to the specific physicochemical properties of the membrane and processing techniques [65,69].

Based on these observations, the present ex vivo and in vivo studies were performed to investigate a collagen membrane derived from bovine Achilles

64

tendon with a specific structural architecture, SYMBIOS®. Histological and histomorphometric analyses of the implantation bed were utilized in the present study to evaluate the cellular responses after biomaterial application at different time points. We particularly focused on the influences of the physiochemical characteristics on the material on the integration, vascularization and cellular inflammatory pattern compared to the physiological wound healing observed in the sham-operation group. In addition, a histomorphometric examination was performed to quantify the histological results. With the aid of a digital camera and a computer with suitable software, various measurements were conducted on the images of the sections. The present study determined the membrane thickness and the number and area of vessels and MNGCs within the implantation beds [70]. The histomorphometric examination enabled the quantification of the histological results, a detailed analysis of the different cells and tissues, and better comparability of the results and statistical analysis [70,71].

In addition to using biomaterials, a variety of regenerative procedures have been employed to promote tissue regeneration. The use of PRF was reported as to be an advantageous, low-cost, biocompatible treatment that exhibited better wound healing properties [51].

Ghanaati et al. further developed PRF by introducing the "low-speed centrifugation concept (LSCC)" for blood to generate i-PRF [50]. Using LSCC, i-PRF is produced by the centrifugation of blood samples at a relatively low centrifugal force to provide high numbers of leukocytes, platelets and growth factors such as transforming growth factor-beta (TGF-ß1) and vascular endothelial growth factor (VEGF), as well as platelet-derived growth factor (PDGF) [49–51]. Moreover, i-PRF is beneficial for clinicians as it can be placed into defects with or without various biomaterials that have been mixed prior to application [51,72].

i-PRF incorporates a liquid fibrinogen matrix with a large number of platelets and leukocyte as well as plasma protein. This concept was established in previous studies by our group and used in an ex vivo model to evaluate the absorbance capacity of collagen membranes [52]. The interaction between i-PRF

and a sugar cross-linked collagen membrane derived from porcine tendon origin revealed the utility of i-PRF, a blood concentrate composed of platelets, leukocytes and growth factors suspended in liquid fibrinogen as a potential tool for investigations of capacity of the biomaterial to absorb plasma proteins and to incorporate human cells. Additionally, some details regarding initial cellular interactions with the biomaterial have been determined using this ex vivo model. Furthermore, in this study, the sugar cross-linked membrane was imperiable to leukocytes and platelets from the i-PRF ex vivo, and similar results were obtained for cellular penetration in vivo [52].

Therefore, in the ex vivo experiments reported in the present study, the evaluation of the membrane permeability of the biomaterial and the initial penetration of human cells into the biomaterial were emphasized using i-PRF. i-PRF was employed to imitate the clinical scenario, in which first contact occurs with components of the peripheral blood following placement of the membrane into the implantation region. Based on the results from the ex vivo experiment in the present study, the biomaterial absorbed i-PRF, showing leukocyte and platelet infiltration throughout the SB. Moreover, a fibrin clot was observed within its porous structure. Therefore, the biomaterial permitted cellular penetration in the early period. In contrast, the application of this method for the evaluation of a sugar cross-linked porcine-derived collagen membrane showed cellular impermeability, as the membrane did not allow the cells and fibrin present in the i-PRF to penetrate into the membrane [52].

Our ex vivo findings are consistent with the in vivo results from the present study, in which histological analysis detected murine inflammatory cells within the biomaterial over the study period of 30 days, without signs of membrane breakdown. Accordingly, the histomophometric analysis of the membrane thickness showed a substantial increase in the SB thickness from days 3 to 10, and the thickness was then maintained. Thus, the SB membrane allowed host cells and connective tissue to enter the membrane body. Simultaneously, the specific membrane structure, such as its pore system and interfibrillar

compartments, provided space for the infiltration of host cells and connective tissue without undergoing biodegradation or disintegration.

The histological analysis of the tissue response to the bovine Achilles tendon-derived SB collagen biomaterial showed that the early cellular reaction to the membrane was mainly represented by mononuclear cells. Three days after implantation, some CD-68-positive macrophages were observed on the SB surface. The mid-term cellular reaction on day 10 was characterized by an increasing number of CD-68-positive cells compared to day 3. Additionally, some MNGCs were observed on the biomaterial surface at this time point, accompanied by significantly increased vascularization. The control group reflects the physiological process of wound healing. MNGCs were not detected in the control group, but a gradual increase in vascularization was observed over time.

At the evaluation of the mid-term cellular reaction on day 15, a different pattern of inflammation was observed. Thereby, macrophages decreased significantly in number compared to day 10, whereas the number of MNGCs was significantly increased. This significant reduction in the number of CD-68 cells on days 10 and 15 in the SB group may be related to different explanations. One explanation may be the life time of macrophages during the wound healing as a physiological process. This is supported by the observation of a decreased number of macrophages also in the control group. Further explanation may be that the persistence of macrophages although in a smaller number than day 10 but still higher than the control group that may be refered to a different macrophages type, that is not only involved in the wound healing but also in the formation of MNGCs [73]. In this process in macrophages undergo fusion to creat MNGCs after fail to phagocytize the implanted foreign biomaterial [74]. These MNGCs possess an enhanced oxidative capacity. Therefore, the dynamic changes observed in the numbers of macrophages and MNGCs in the present study might have been due to their fusion and the process of MNGC formation.

At the last observation time point on day 30, the numbers of macrophages and MNGCs did not show significant changes. These findings were similar to the

rate of vascularization, which did not exhibit significant changes after day 10. One interesting finding was the interrelation the number of MNGCs and the vascularization rate. Both increased significantly from day 3 to 15 alike. The presence of MNGCs might explain the substantial increase in the vascularization of the peri-implanted region, as these cells have the potential to express proangiogenic signal molecules (VEGF), which apparently contributes to increased vascularization in the implantation bed [75,76]. MNGCs and vascularization were similarly observed within the implantation beds of different biomaterials, including synthetic and xenogeneic bone substitute materials and membranes, in previous studies [54,75–77]. Based on the data from the present study, the formation of MNGCs and enhanced vascularization are circumstantial evidence of a foreign body reaction [78,79].

MNGCs are an indication of a foreign body reaction to several biomaterials, including collagen-based biomaterials [54], silk-based polymers [80] and different synthetic and xenogeneic bone substitute materials[81]. However, the biomaterial-induced MNGCs share common characteristics with disease-related MNGCs (Langerhans' MNGCs) present in patients with tuberculosis and sarcoidosis, such as morphology, the number of nuclei, and the expression of surface proteins (e.g., CD-68, Integrin β1/2 and HLA-DR) [74]. Therefore, a remaining question is whether the presence of MNGCs should be accepted as a biomaterial-induced cellular reaction or an adverse reaction.

In the simulated physiological wound healing in the control group employed of this study, mild vascularization without an appearance of MNGCs was detected. Several biomaterials, such as noncross-linked bilayer porcine dermis- and peritoneum-derived collagen membranes, have been reported to elicit a physiological mononuclear cell reaction and maintain their initial structure throughout the study time of 60 days. This collagen matrix allowed slow penetration into the biomaterial superficial layer but served as a functional barrier within its central region and allowed integration within the host tissue [53]. In contrast, the SB membrane allowed the host mononuclear cells to gradually

penetrate towards the membrane central region without undergoing disintegration until a later time point. MNGCs were detected only on the biomaterial interface and were not able to enter the membrane body, similar to neo-vessels. The vascularization was merely enhanced in the peri-implanted area.

Notably, two different inflammatory responses, mononuclear cells and MNGCs, were induced by the SB. This specific inflammatory pattern may be beneficial in recruiting the vasculature to the implantation region without causing any signs of membrane breakdown. This effect might be explained by the membrane-specific architecture of the biomaterial, namely, a loose structure with detectable porosity, which allowed the mononuclear cells to migrate into the center region and integrate within the biomaterial to prevent over-accumulation on the surface, resulting in a lower number of MNGCs. Additionally, despite the presence of MNGCs, the SB membrane maintained its integrity over 30 days and allowed only mononuclear cells to enter its central region while resisting the MNGCs. Additionally, no signs of degradation were detected over the evaluation time period. Studies aiming to elucidate whether the presence of MNGCs will lead to a classical foreign body reaction and encapsulation of the biomaterial or whether these cells would provide any contribution to the degradation process of the biomaterial leading to its resorption will be interesting.

However, the porcine-derived non-cross-linked collagen-based biomaterial induced a foreign body reaction, as the biomaterial induced the formation of MNGCs and vessel-rich granulation tissue in combination with disintegration by premature ingrowth of the peri-implanted connective tissue [54,55]. In contrast, the bovine-origin biomaterial used in the present study did not exhibit signs of premature breakdown or disintegration in terms of loss of the native structure until the later phase of the study. Various animal-derived collagens harvested from specific compartments might elicit different levels of pro-inflammatory reactions. Moreover, the use of different manufacturing procedures and purification methods might change the surface characteristics of the native collagen structure in the biomaterial, which would result in different biomaterial degradation or host tissue

integration patterns.[54,82] However, an additional long-term study is required to determine the cellular reaction and the consequences of inducing MNGCs, to understand the degradation pattern of this resorbable biomaterial, and to overcome the limitations of the present study.

Another naturally derived biomaterial composed of silk fibroin exhibited a membrane-induced formation of MNGCs and transmembrane vascularization, as well as a breakdown of the membrane integrity after 60 days. However, silk fibroin induced only the formation of TRAP-positive MNGCs, which suggests pro-inflammatory activity [28] In contrast, in the present study, we mainly observed TRAP-negative MNGCs, which might represent a different MNGC type, as the biomaterial remained an intact barrier. This difference might affect the host cellular response through subsequent polarization of macrophages and alterations in their cytokine expression patterns, which might influence their fusion into MNGCs [82,83]. However, further studies are needed to determine the interplay between differentially activated macrophages and the formation of MNGCs in an attempt to obtain more in-depth knowledge of mononuclear cell and MNGC activation and polarization.

Finally, the appearance of MNGCs on the SB interfaces, which reflects a foreign body reaction to the biomaterial, did not lead to a loss of membrane integrity. Based on the observed results, the SB membrane might exert a beneficial effect on the regenerative ability of the penetrating host cells instead of a scaffold serving to promote tissue regeneration in GTR. Interestingly, in an animal study using a tooth dehiscence model for periodontological regeneration, the capability of a bovine Achilles tendon-derived collagen biomaterial to regenerate the lost periodontal apparatus was comparable to a noncross-linked porcine-derived collagen membrane, which resulted in a significant increase in bone formation and connective tissue attachment [36]. Furthermore, according to a clinical study, bovine-derived collagen membranes are suitable for successful root coverage as a scaffold and good recipient connective tissue integration [34].

Additionally, further investigations based on the present findings are necessary to elucidate the types of biomaterial-related MNGCs, the molecular mechanisms by which MNGCs contribute to the regenerative process induced by biomaterials and whether MNGCs should be accepted as a physiological reaction or considered a pathological reaction. Currently, numerous biomaterials are available for clinicians to use in GTR/GBR. However, the clinical suitability of different biomaterials for each tissue and each patient is very important. These findings are highly clinically interesting for an evaluation of the clinical suitability of different biomaterials and definition of suitable indications with respect to the physicochemical properties of the biomaterial.

5. Conclusion

The present study was designed to analyze the cellular reaction to a novel collagen membrane derived from bovine Achilles tendon. The biomaterial permitted cellular penetration in the early period ex vivo, as evidenced by the leukocyte and platelet infiltration throughout the collagen membrane and the presence of a fibrin clot within its porous structure.

Histologically, the membrane preserved its native structure over 30 days without undergoing disintegration. Moreover, the tissue response showed an initial reaction of mononuclear cells and induced MNGCs beginning on day 10, whereas no MNGCs were detected within the control group that reflected the physiological process of wound healing. Afterwards, the macrophage number, which was detected by CD-68 staining, was significantly decreased compared to day 10. However, the number of MNGCs was significantly increased compared to day 10, indicating that macrophages had fused to form MNGCs, which were only located on the membrane surface. The presence of MNGCs was accompanied by a significant increase in the vascularization in the peri-implantation area. No signs of transmembrane vascularization was detected. MNGCs were detected only on the biomaterial interface. These cells were mainly TRAP-negative MNGCs that were not able to enter the membrane body over the study period. These characteristics indicated a foreign body reaction to the biomaterial surface. However, the role of the MNGCs induced by this biomaterial requires further investigation. Furthermore, the biomaterial absorbed proteins and allowed cells to penetrate its central region following the application of i-PRF ex vivo. Hence, the increase in thickness reflects the capacity of the membrane to incorporate the host cells and connective tissue to form a scaffold without undergoing any signs of breakdown or disintegration in vivo. Based on these findings, further studies are needed to investigate whether the occurrence of MNGCs represents a physiological biomaterial-related cellular reaction or an adverse reaction.

6. Zusammenfassung

Die vorliegende Studie hatte das Ziel, die Gewebereaktion von Symbios® resorbierbarer Kollagenmembran SR, welches von der Achillessehne aus Rindern stammt, mit der physiologischen Wundheilung als Kontrollstudie zu vergleichen.

Anhand einer Ex-vivo-Analyse wurde unter Verwendung von injizierbaren Plättchen-reichem Fibrin versucht, die Membranpermeabilität und die Wechselwirklungen mit menschlichen Zellen und Plasmaproteinen zu untersuchen. Das injizierbare Plättchem-reiche Fibrin ist dabei ein Blutkonzentrat, das von zentrifugiertem menschlichem peripherem Blut stammt und zusätzlich Fibrin, Leukozyten und Blutplättchen enthält. In einer In-vivo-Tierstudie bei Wistar-Ratten erfolgte die subkutane Implantation von Symbios, um die zelluläre Reaktion bis zu 30 Tage nach erfolgter Membranimplantation zu bewerten. Dabei wurden auf histochemischer, immunhistochemischer und histomorphometrischer Ebene Analysen durchgeführt, um die zelluläre Entzündungsreaktion, das Vaskularisierungsmuster und die jeweilige Zellinfiltratonsfähigkeit zu bestimmen.

Im Ex-vivo-Teil der Studie konnte die Kollegenmembran nach 15 Minuten von Leukozyten, Plättchen und Fibrin aus dem i-PRF penetriert werden. Innerhalb der ersten drei Tage der Beobachtungszeit konnten nur mononukleäre Zellen beobachtet werden. 10 Tage später konnten multinukleäre Riesenzellen (MNGCs) in der Kollagenmembran induziert werden. Eine hohe Anzahl von CD-68-positiven Zellen (Makrophagen) konnte ab dem 3. Tag nachgewiesen werden, welche bis zum 30. Tag jedoch wieder abnahm. Zusammen mit der Reduktion der CD-68-positiven Zellen nahm die Anzahl der MNGCs signifikant zu. Die Anwesenheit von MNGCs zeigte auch eine signifikant erhöhte Vaskularisierungsdichte. Innerhalb der zentralen Region der Membran dagegen, wurden nur mononukleäre Zellen (MNCs) ohne jegliche Vaskularisierungen beobachtet. Die Kontrollgruppe spiegelte den physiologischen Prozess der Wundheilung wider, da keine Bildung von MNGCs über 30 Tage beobachtet wurde, zusammen mit einer signifikant niedrigeren Vaskularisierung, verglichen mit der Testgruppe.

Die Ergebnisse spiegelten dabei die dynamischen Veränderungen der zellulären Reaktion, welche die Beziehung zwischen der Makrophagenfusion und der MNGCs-Bildung, sowie die Vaskularisierung im Bereich der Kollagenmembran auf eine Fremdkörperreaktion zeigten. Die Kollagenmembran konnte ihre Struktur und Integrität über die Zeit beibehalten, indem sie aufgrund ihrer spezifischen Porositätsmembranstruktur keine Anzeichen eines vorzeitigen Zusammenbruchs und Zerfalls zeigte.

In diesem Sinne muss hinterfragt werden, ob die Biomaterial-induzierten MNGCs als eine Biomaterial-induzierte zelluläre Reaktion akzeptiert werden kann, welche in der Lage ist, eine Vaskularisation zu induzieren oder eher als Nebenwirkung zu betrachten. Daher sind umfangreiche präklinische und klinische Studien notwendig, um die Art von MNGCs zu untersuchen, die durch dieses spezifische Membranmaterial hervorgerufen werden.

7. Summary

The present study aimed to assess the tissue response to the SYMBIOS® resorbable collagen membrane SR, which is derived from bovine Achilles tendon, and compare it to the physiological wound healing of a sham operation as a control.

An ex vivo analysis was performed using injectable platelet-rich fibrin (i-PRF), that is gained by the centrifugation of human venous blood and contains fibrin, leukocytes and platelets, to elucidate the membrane permeability and interactions with human cells and plasma proteins. In the in vivo study, a subcutaneous implantation model was established in Wistar rats to evaluate the cellular reactions for up to 30 days after membrane implantation. Histochemical, immunohistochemical and histomorphometric analyses were performed to assess the cellular inflammatory response, vascularization pattern and cell infiltration capacity.

In the ex vivo study, i-PRF components including fibrin, leukocytes and platelets penetrated the membrane after just 15 minutes. Within the observation period, the cellular reaction in the early phase, which included the first 3 days, produced only mononuclear cells. From 10 to 30 days , the formation of multinucleated giant cells (MNGCs) was induced by the collagen membrane. CD-68 positive cells (macrophages) occurred in a high number on day 3, and the number decreased over time up to day 30. Along with the reduction in the number of CD-68 positive cells, the number of MNGCs increased significantly. The presence of MNGCs was accompanied by significantly increased vascularization within the central region of the membrane, and only mononuclear cells (MNCs) did not produce vascularization. In contrast, the accumulated MNGCs were located on the membrane surface. The control group reflected the physiological process of wound healing, as MNGCs did not form over the 30 day period, and a significantly lower level of vascularization was observed compared with the test group.

This finding showed dynamic changes in the cellular reaction, which indicated a relationship between macrophage fusion and MNGC formation, and vascularization of the collagen membrane is circumstantial evidence of a reaction to a foreign body. However, the collagen membrane was able to maintain its structure and integrity over time, showing no signs of premature breakdown and disintegration due to the specific porosity of its membrane structure.

Therefore, we questioned whether the biomaterial-induced formation of MNGCs should be accepted as a biomaterial-induced cellular reaction that is able to restore vascularization or as an adverse reaction. Therefore, extensive preclinical and clinical studies are needed to investigate the type of MNGCs that form in response to the membrane material studied here.

8. Reference

1.   Ghanaati S, Kirkpatrick C, Kovács A, et al. Synthetic bone substitute material comparable with xenogeneic material for bone tissue regeneration in oral cancer patients: First and preliminary histological, histomorphometrical and clinical results. *Ann Maxillofac Surg*. 2013;3(2):126. doi:10.4103/2231-0746.119221.

2.   Chiapasco M, Colletti G, Romeo E, Zaniboni M, Brusati R. Long-term results of mandibular reconstruction with autogenous bone grafts and oral implants after tumor resection. *Clin Oral Implants Res*. 2008;19(10):1074-1080. doi:10.1111/j.1600-0501.2008.01542.x.

3.   Araujo MG, Lindhe J. Dimensional ridge alterations following tooth extraction. An experimental study in the dog. *J Clin Periodontol*. 2005;32(2):212-218. doi:10.1111/j.1600-051X.2005.00642.x.

4.   Tallgren A. The continuing reduction of the residual alveolar ridges in complete denture wearers: a mixed-longitudinal study covering 25 years. 1972. *J Prosthet Dent*. 2003;89(5):427-435. doi:10.1016/S0022391303001586.

5.   Jun C-M, Yun J-H. Three-Dimensional Bone Regeneration of Alveolar Ridge Defects Using Corticocancellous Allogeneic Block Grafts: Histologic and Immunohistochemical Analysis. *Int J Periodontics Restorative Dent*. 2016;36(1):75-81. doi:10.11607/PRD.1950.

6.   Barrowman R, Wilson P, Wiesenfeld D. Oral rehabilitation with dental implants after cancer treatment. *Aust Dent J*. 2011;56(2):160-165. doi:10.1111/j.1834-7819.2011.01318.x.

7.   Dahlin C, Sennerby L, Lekholm U, Linde A, Nyman S. Generation of new bone around titanium implants using a membrane technique: an experimental study in rabbits. *Int J Oral Maxillofac Implants*. 1989;4(1):19-25. http://www.ncbi.nlm.nih.gov/pubmed/2599578. Accessed February 15, 2018.

8.   Dahlin C, Linde A, Gottlow J, Nyman S. Healing of bone defects by guided tissue regeneration. *Plast Reconstr Surg*. 1988;81(5):672-676. http://www.ncbi.nlm.nih.gov/pubmed/3362985. Accessed February 15, 2018.

9.   Gher ME, Quintero G, Assad D, Monaco E, Richardson AC. Bone Grafting and Guided Bone Regeneration for Immediate Dental Implants in Humans. *J Periodontol*. 1994;65(9):881-891. doi:10.1902/jop.1994.65.9.881.

10.   Lang NP, Hämmerle CH, Brägger U, Lehmann B, Nyman SR. Guided tissue regeneration in jawbone defects prior to implant placement. *Clin Oral Implants Res*. 1994;5(2):92-97. http://www.ncbi.nlm.nih.gov/pubmed/7918914. Accessed February 15, 2018.

11.   Liu J, Kerns DG. Mechanisms of guided bone regeneration: a review. *Open Dent J*. 2014;8:56-65. doi:10.2174/1874210601408010056.

12.   Araujo MG, Lindhe J. Dimensional ridge alterations following tooth extraction. An experimental study in the dog. *J Clin Periodontol*. 2005;32(2):212-218. doi:10.1111/j.1600-051X.2005.00642.x.

13.   Cawood JI, Howell RA. A classification of the edentulous jaws. *Int J Oral Maxillofac Surg*. 1988;17(4):232-236. doi:10.1016/S0901-5027(88)80047-X.

14.   Solar, P.; Aro, G.; Ulm, C.; Bernhart T. Die Auswirkungen des Zahnverlustes auf die Anatomie der Maxilla. *Schweiz Monatsschr Zahnmed 108 (9), S 871–878*. 1998.

15.   Bottino MC, Thomas V, Schmidt G, et al. Recent advances in the development of GTR/GBR membranes for periodontal regeneration—A materials perspective. *Dent Mater*. 2012;28(7):703-721. doi:10.1016/j.dental.2012.04.022.

16.   Koeck B. *Implantologie*. 2. Auflage. Urban & Fischer Verlag/Elsevier GmbH; 2005.

17.   Atwood DA, Coy WA. Clinical, cephalometric, and densitometric study of reduction of residual ridges. *J Prosthet Dent*. 1971;26(3):280-295. doi:10.1016/0022-3913(71)90070-9.

18.   Isaksson S, Alberius P. Maxillary alveolar ridge augmentation with onlay bone-grafts and immediate endosseous implants. *J Craniomaxillofac Surg*. 1992;20(1):2-7. http://www.ncbi.nlm.nih.gov/pubmed/1564115. Accessed February 17, 2018.

19.   SCHROPP L, ISIDOR F. Timing of implant placement relative to tooth extraction. *J Oral Rehabil*. 2008;35(s1):33-43. doi:10.1111/j.1365-2842.2007.01827.x.

20.   Fugazzotto PA. Simplified technique for immediate implant insertion into extraction sockets: report of technique and preliminary results. *Implant Dent*. 2002;11(1):79-82. http://www.ncbi.nlm.nih.gov/pubmed/11915550. Accessed February 17, 2018.

21.   Misch CE, Dietsh F. Bone-grafting materials in implant dentistry. *Implant Dent*. 1993;2(3):158-167. http://www.ncbi.nlm.nih.gov/pubmed/8142935. Accessed February 17, 2018.

22.   Damien CJ, Parsons JR. Bone graft and bone graft substitutes: A review of current technology and applications. *J Appl Biomater*. 1991;2(3):187-208. doi:10.1002/jab.770020307.

23.   Younger EM, Chapman MW. MORBIDITY AT BONE GRAFT DONOR SITES. *Repr from J Orthop TRAUMA*. 3(3):192-195. https://pdfs.semanticscholar.org/baa6/a455d8f36a7d95ff8833167f74a2a31f64e2.pdf. Accessed February 17, 2018.

24.   Conrad EU, Gretch DR, Obermeyer KR, et al. Transmission of the hepatitis-C virus by tissue transplantation. *J Bone Joint Surg Am*. 1995;77(2):214-224. http://www.ncbi.nlm.nih.gov/pubmed/7844127. Accessed February 17, 2018.

25.   Emam HA, Stevens MR. Concepts in Bone Reconstruction for Implant Rehabilitation. In: Motamedi MHK, ed. *A Textbook of Advanced Oral and Maxillofacial Surgery*. ; 2013:617-640. doi:10.5772/53401.

26.   Aghaloo TL, Moy PK. Which hard tissue augmentation techniques are the most successful in furnishing bony support for implant placement? *Int J Oral Maxillofac Implants*. 2007;22 Suppl:49-70. http://www.ncbi.nlm.nih.gov/pubmed/18437791. Accessed February 17, 2018.

27.   Rakhmatia YD, Ayukawa Y, Furuhashi A, Koyano K. Current barrier membranes: Titanium mesh and other membranes for guided bone regeneration in dental applications. *J Prosthodont Res*. 2013;57(1):3-14. doi:10.1016/J.JPOR.2012.12.001.

28.   Ghanaati S. Non-cross-linked porcine-based collagen I-III membranes do not require high vascularization rates for their integration within the implantation bed: A paradigm shift. *Acta Biomater*. 2012;8(8):3061-3072. doi:10.1016/j.actbio.2012.04.041.

29.   Scantlebury T V. 1982-1992: A Decade of Technology Development for Guided Tissue Regeneration. *J Periodontol*. 1993;64(11s):1129-1137. doi:10.1902/jop.1993.64.11s.1129.

30.   Salzmann DL, Kleinert LB, Berman SS WS. The effects of porosity on endothelialization of ePTFE implanted in subcutaneous and adipose tissue. *J Biomed Mater Res*. 1997;34:463–76.

31.   Kostopoulos L, Karring T. Augmentation of the rat mandible using guided tissue regeneration. *Clin Oral Implants Res*. 1994;5(2):75-82. doi:10.1034/j.1600-0501.1994.050203.x.

32.   Heinze J. A Space-maintaining Resorbable Membrane for Guided Tissue Regeneration. *Most*. 2004;(1998):1-4.

33.   Lorenz J, Blume M, Barbeck M, et al. Expansion of the peri-implant attached gingiva with a three-dimensional collagen matrix in head and neck cancer patients—results from a prospective clinical and histological study. *Clin Oral Investig*. 2017;21(4):1103-1111. doi:10.1007/s00784-016-1868-2.

34.   Schlee M, Ghanaati S, Willershausen I, Stimmlmayr M, Sculean A, Sader RA. Bovine pericardium based non-cross linked collagen matrix for successful root coverage, a clinical study in human. *Head Face Med*. 2012;8(1):6. doi:10.1186/1746-160X-8-6.

35.   Ghanaati S, Kovács A, Barbeck M, et al. Bilayered, non-cross-linked

collagen matrix for regeneration of facial defects after skin cancer removal: a new perspective for biomaterial-based tissue reconstruction. *J Cell Commun Signal*. 2016;10(1):3-15. doi:10.1007/s12079-015-0313-7.

36. Behfarnia P, Khorasani MM, Birang R, Abbas FM. Histological and histomorphometric analysis of animal experimental dehiscence defect treated with three bio absorbable GTR collagen membrane. *Dent Res J (Isfahan)*. 2012;9(5):574-581. http://www.ncbi.nlm.nih.gov/pubmed/23559922. Accessed February 17, 2018.

37. Ehmke B, Rüdiger SG, Hommens A, Karch H, Flemmig TF. Guided tissue regeneration using a polylactic acid barrier. *J Clin Periodontol*. 2003;30(4):368-374. http://www.ncbi.nlm.nih.gov/pubmed/12694438. Accessed February 17, 2018.

38. Polimeni G, Albandar JM, Wikesjö UME. Prognostic factors for alveolar regeneration: Effect of space provision. *J Clin Periodontol*. 2005;32(9):951-954. doi:10.1111/j.1600-051X.2005.00763.x.

39. Kawasaki T, Ohba S, Nakatani Y, Asahina I. Clinical study of guided bone regeneration with resorbable polylactide-co-glycolide acid membrane. *Odontology*. 2018;(123456789):1-6. doi:10.1007/s10266-018-0349-2.

40. Sculean A, Nikolidakis D, Schwarz F. Regeneration of periodontal tissues: Combinations of barrier membranes and grafting materials - Biological foundation and preclinical evidence: A systematic review. *J Clin Periodontol*. 2008;35(SUPPL. 8):106-116. doi:10.1111/j.1600-051X.2008.01263.x.

41. Minichetti JC, D'Amore JC, Hong AYJ, Cleveland DB. Human Histologic Analysis of Mineralized Bone Allograft (Puros) Placement Before Implant Surgery. *J Oral Implantol*. 2004;30(2):74-82. doi:10.1563/0.693.1.

42. Salamanca E, Tsai C-Y, Pan Y-H, et al. In Vitro and In Vivo Study of a Novel Porcine Collagen Membrane for Guided Bone Regeneration. *Materials (Basel)*. 2016;9(11):949. doi:10.3390/ma9110949.

43. T. Velnar, T. Bailey VS. The wound healing process: an overview of the cellular and molecular mechanisms. *J Int Med Res*. 2009;37(375):1528–1542.

44. Robson MC, Steed DL, Franz MG. Wound Healing: Biologic Features and Approaches to Maximize Healing Trajectories. *Curr Probl Surg*. 2001;38(2):1-140. doi:10.1067/j.cpsurg.2008.10.004.

45. Singh S, Young A, McNaught CE. The physiology of wound healing. *Surg (United Kingdom)*. 2017;35(9):473-477. doi:10.1016/j.mpsur.2017.06.004.

46. Attinger GBJEJCE. The Basic Science of Wound Healing. *Plast Reconstr Surgery 117(7S)12S-34S*.

47. Pierce GF, Mustoe TA, Altrock BW, Deuel TF, Thomason A. Role of

Platelet-Derived Growth Factor in Wound Healing. 1991;326:319-326.

48.   Phases of Wound Healing- Part 1 | WoundEducators.com.
https://woundeducators.com/phases-of-wound-healing/. Accessed February
22, 2018.

49.   Choukroun J, Ghanaati S. Reduction of relative centrifugation force within
injectable platelet-rich-fibrin (PRF) concentrates advances patients' own
inflammatory cells, platelets and growth factors: the first introduction to the
low speed centrifugation concept. *Eur J Trauma Emerg Surg*. 2018;44(1):87-
95. doi:10.1007/s00068-017-0767-9.

50.   Ghanaati S, Booms P, Orlowska A, et al. Advanced Platelet-Rich Fibrin: A
New Concept for Cell-Based Tissue Engineering by Means of Inflammatory
Cells. *J Oral Implantol*. 2014;40(6):679-689. doi:10.1563/aaid-joi-D-14-
00138.

51.   Miron RJ, Fujioka-Kobayashi M, Hernandez M, et al. Injectable platelet rich
fibrin (i-PRF): opportunities in regenerative dentistry? *Clin Oral Investig*.
2017;21(8):2619-2627. doi:10.1007/s00784-017-2063-9.

52.   Chia-Lai P ju, Orlowska A, Al-Maawi S, et al. Sugar-based collagen
membrane cross-linking increases barrier capacity of membranes. *Clin Oral
Investig*. 2017:1-13. doi:10.1007/s00784-017-2281-1.

53.   Ghanaati S, Schlee M, Webber MJ, et al. Evaluation of the tissue reaction to
a new bilayered collagen matrix in vivo and its translation to the clinic.
Biomed Mater. 2011;6(1):15010. doi:10.1088/1748-6041/6/1/015010.

54.   Barbeck M, Lorenz J, Kubesch A, et al. Porcine Dermis-Derived Collagen
Membranes Induce Implantation Bed Vascularization Via Multinucleated
Giant Cells: A Physiological Reaction? *J Oral Implantol*. 2015;41(6):e238-
e251. doi:10.1563/aaid-joi-D-14-00274.

55.   Barbeck M, Lorenz J, Holthaus MG, et al. Porcine Dermis and Pericardium-
Based, Non-Cross-Linked Materials Induce Multinucleated Giant Cells After
Their In Vivo Implantation: A Physiological Reaction? *J Oral Implantol*.
2015;41(6):e267-81. doi:10.1563/aaid-joi-D-14-00155.

56.   Lorenz J, Kubesch A, Korzinskas T, et al. TRAP-Positive Multinucleated
Giant Cells Are Foreign Body Giant Cells Rather Than Osteoclasts: Results
From a Split-Mouth Study in Humans. *J Oral Implantol*. 2015;41(6):e257-
e266. doi:10.1563/AAID-JOI-D-14-00273.

57.   Barbeck M, Motta A, Migliaresi C, Sader R, Kirkpatrick CJ, Ghanaati S.
Heterogeneity of biomaterial-induced multinucleated giant cells: Possible
importance for the regeneration process? *J Biomed Mater Res - Part A*.
2016;104(2):413-418. doi:10.1002/jbm.a.35579.

58.   Kiernan JA (John A. *Histological and Histochemical Methods : Theory and
Practice*. Oxford [U.K.] ; Boston : Butterworth-Heinemann; 1999.

59. Goldner J. A modification of the masson trichrome technique for routine laboratory purposes. *Am J Pathol*. 1938;14(2):237-243. http://www.ncbi.nlm.nih.gov/pubmed/19970387. Accessed February 23, 2018.

60. Revell PA. Review article Histomorphometry of bone. 1983:1323-1331.

61. Al-Maawi S, Vorakulpipat C, Orlowska A, Zrc T, Sader RA, Kirkpatrick CJ, Ghanaati S. In vivo implantation of a bovine-derived collagen membrane leads to changes in the physiological cellular pattern of wound healing by the induction of multinucleated giant cells: An adverse reaction *FrontBioengBiotechnol*. 2018.

62. Needleman I, Worthington H V., Giedrys-Leeper E, Tucker R. Guided tissue regeneration for periodontal intrabony defects – a Cochrane Systematic Review. *Cochrane Database Syst Rev*. 2006;37(2):106-123. doi:10.1002/14651858.CD001724.pub2.www.cochranelibrary.com.

63. Fuchs S, Jiang X, Schmidt H, et al. Dynamic processes involved in the pre-vascularization of silk fibroin constructs for bone regeneration using outgrowth endothelial cells. *Biomaterials*. 2009;30(7):1329-1338. doi:10.1016/j.biomaterials.2008.11.028.

64. Fuchs S, Ghanaati S, Orth C, et al. Contribution of outgrowth endothelial cells from human peripheral blood on in vivo vascularization of bone tissue engineered constructs based on starch polycaprolactone scaffolds. *Biomaterials*. 2009;30(4):526-534. doi:10.1016/j.biomaterials.2008.09.058.

65. Bunyaratavej P, Wang H-L. Collagen Membranes: A Review. *J Periodontol*. 2001;72(2):215-229. doi:10.1902/jop.2001.72.2.215.

66. Hsu FY, Chueh SC, Wang YJ. Microspheres of hydroxyapatite/reconstituted collagen as supports for osteoblast cell growth. *Biomaterials*. 1999;20(20):1931-1936. http://www.ncbi.nlm.nih.gov/pubmed/10514070. Accessed March 18, 2017.

67. Gamal AY, Iacono VJ. Enhancing Guided Tissue Regeneration of Periodontal Defects by Using a Novel Perforated Barrier Membrane. *J Periodontol*. 2013;84(7):905-913. doi:10.1902/jop.2012.120301.

68. Di Stefano DA, Andreasi Bassi M, Cinci L, Pieri L, Ammirabile G. Treatment of a bone defect consequent to the removal of a periapical cyst with equine bone and equine membranes: clinical and histological outcome. *Minerva Stomatol*. 61(11-12):477-490. http://www.ncbi.nlm.nih.gov/pubmed/23207673. Accessed March 15, 2018.

69. Ghanaati S, Barbeck M, Detsch R, et al. The chemical composition of synthetic bone substitutes influences tissue reactions *in vivo*: histological and histomorphometrical analysis of the cellular inflammatory response to hydroxyapatite, beta-tricalcium phosphate and biphasic calcium phosphate ceramics. *Biomed Mater*. 2012;7(1):15005. doi:10.1088/1748-

6041/7/1/015005.

70.   Ghanaati S, Orth C, Unger RE, et al. Fine-tuning scaffolds for tissue regeneration: effects of formic acid processing on tissue reaction to silk fibroin. *J Tissue Eng Regen Med*. 2010;4(6):n/a-n/a. doi:10.1002/term.257.

71.   Ghanaati S, Webber MJ, Unger RE, et al. Dynamic in vivo biocompatibility of angiogenic peptide amphiphile nanofibers. *Biomaterials*. 2009;30(31):6202-6212. doi:10.1016/j.biomaterials.2009.07.063.

72.   Melek LN, El Said MM. Evaluation of "Autogenous Bioengineered Injectable PRF – Tooth graft" combination (ABIT) in reconstruction of maxillary alveolar ridge defects: CBCT volumetric analysis. *Saudi J Dent Res*. 2017;8(1-2):86-96. doi:10.1016/J.SJDR.2016.10.005.

73.   MacLauchlan S, Skokos EA, Meznarich N, et al. Macrophage fusion, giant cell formation, and the foreign body response require matrix metalloproteinase 9. *J Leukoc Biol*. 2009;85(4):617-626. doi:10.1189/jlb.1008588.

74.   Al-Maawi S, Orlowska A, Sader R, James Kirkpatrick C, Ghanaati S. In vivo cellular reactions to different biomaterials—Physiological and pathological aspects and their consequences. *Semin Immunol*. 2017;29(February):49-61. doi:10.1016/j.smim.2017.06.001.

75.   Ghanaati S, Barbeck M, Orth C, et al. Influence of β-tricalcium phosphate granule size and morphology on tissue reaction in vivo. *Acta Biomater*. 2010;6(12):4476-4487. doi:10.1016/j.actbio.2010.07.006.

76.   Ghanaati S, Unger RE, Webber MJ, et al. Scaffold vascularization in vivo driven by primary human osteoblasts in concert with host inflammatory cells. *Biomaterials*. 2011;32(32):8150-8160. doi:10.1016/J.BIOMATERIALS.2011.07.041.

77.   Barbeck M, Udeabor S, Lorenz J, et al. High-Temperature Sintering of Xenogeneic Bone Substitutes Leads to Increased Multinucleated Giant Cell Formation: In Vivo and Preliminary Clinical Results. *J Oral Implantol*. 2015;41(5):e212-e222. doi:10.1563/aaid-joi-D-14-00168.

78.   Anderson JM, Jones JA. Phenotypic dichotomies in the foreign body reaction. *Biomaterials*. 2007;28(34):5114-5120. doi:10.1016/j.biomaterials.2007.07.010.

79.   McNally AK, Anderson JM. Phenotypic expression in human monocyte-derived interleukin-4-induced foreign body giant cells and macrophages in vitro: dependence on material surface properties. *J Biomed Mater Res A*. 2015;103(4):1380-1390. doi:10.1002/jbm.a.35280.

80.   Ghanaati S, Orth C, Unger RE, et al. Fine-tuning scaffolds for tissue regeneration: effects of formic acid processing on tissue reaction to silk fibroin. *J Tissue Eng Regen Med*. 2010;4(6):n/a-n/a. doi:10.1002/term.257.

81. Ghanaati S, Orth C, Barbeck M, et al. Histological and histomorphometrical analysis of a silica matrix embedded nanocrystalline hydroxyapatite bone substitute using the subcutaneous implantation model in Wistar rats. *Biomed Mater*. 2010;5(3):35005. doi:10.1088/1748-6041/5/3/035005.

82. Jones JA, Dadsetan M, Collier TO, et al. Macrophage behavior on surface-modified polyurethanes. *J Biomater Sci Polym Ed*. 2004;15(5):567-584.

83. Kajahn J, Franz S, Rueckert E, et al. Artificial extracellular matrices composed of collagen I and high sulfated hyaluronan modulate monocyte to macrophage differentiation under conditions of sterile inflammation. *Biomatter*. 2012;2(4):226-236. doi:10.4161/biom.22855.

84. Reich K, Huber C, Lippnig W, Ulm C, Watzek G, Tangl S. Atrophy of the residual alveolar ridge following tooth loss in an historical population. *Oral Dis*. 2011;17(1):33-44. doi:10.1111/j.1601-0825.2010.01699.x.

9. Acknowledgments

10. Lebenslauf

Persönliche Daten

Name	Chakorn Vorakulpipat
Wohnhaft	161/29 Prapinklao Road, Bangkoknoi, Bangkok, Thailand 10700
E-Mail	chakorn.vor@mahidol.ac.th
	chakorn@gmx.de
Geburtsdatum	08.03.1981
Geburtsort	Bangkok, Thailand
Staatsangehörigkeit	thailändisch
Familienstand	verheiratet, 1 Kind

Schulbildung

05/1993 – 03/1998	Debsirin Gymnasium, Bangkok
05/1987 – 03/1993	Grundschule Thewphaingarm, Bangkok

Studium und Beruf

05/2018	Anerkennung als Facharzt für Mund-, Kiefer- und Gesichtschirurgie
02/2015	Deutsche Approbation als Zahnarzt, Landeszahnärztekammer, Hessen
01/2014	Deutsche Approbation als Arzt, Landesärztekammer, Hessen
04/2009	Befähigung in Allgemeiner Heilkunde Der Medizinische Rat, Thailand

03/2009	Abschluss : Diplom der Humanmedizin, Thailand
05/2004 – 03/2009	Studium der Humanmedizin in Siriraj Krankenhaus, Bangkok, Thailand
03/2004	Befähigung in Allgemeiner Zahnheilkunde Der Zahnmedizinische Rat, Thailand
03/2004	Abschluss : Diplom der Zahnmedizin
05/1998 – 03/2004	Studium der Zahnmedizin, an der Mahidol Universität, Bangkok

Praktikum

07.09.2010 - 05.11.2010	Praktikum in der Klinik für Mund-, Kiefer und Plastische Gesichtschirurgie, Universitätsklinikum, Frankfurt am Main

Berufliche Tätigkeiten

Seit 01.10.2011	Weiterbildung zum Mund Kiefer Gesichtschirurg, Universitätsklinikum Frankfurt am Main, Klinik für Mund-, Kiefer- und plastische Gesichtschirurgie, Direktor: Prof. Dr. Dr. Dr. Sader
05/2009 – 03/2011	Notarzt, Srivichai Krankenhaus, Bangkok
04/2004 – 03/2009	Zahnarzt in der Klinik für Mund-, Kiefer- und Gesichtschirurgie, Mahidol Universität, Thailand

Frankfurt am Main, 30.05.2018

11. Schriftliche Erklärung

Ich erkläre ehrenwörtlich, dass ich die dem Fachbereich Medizin der Johann Wolfgang Goethe-Universität Frankfurt am Main zur Promotionsprüfung eingereichte Dissertation mit dem Titel

Ex vivo and in vivo analysis of tissue reaction towards collagen membrane (Symbios)

in der Klinik für Mund- Kiefer- und Plastische Gesichtschirurgie unter Betreuung und Anleitung von Prof. Dr. Dr. Dr. Shahram Ghanaati ohne sonstige Hilfe selbst durchgeführt und bei der Abfassung der Arbeit keine anderen als die in der Dissertation angeführten Hilfsmittel benutzt habe. Darüber hinaus versichere ich, nicht die Hilfe einer kommerziellen Promotionsvermittlung in Anspruch genommen zu haben.

Ich habe bisher an keiner in- oder ausländischen Universität ein Gesuch um Zulassung zur Promotion eingereicht.

Die vorliegende Arbeit wurde bisher nicht als Dissertation eingereicht.

Vorliegende Ergebnisse der Arbeit wurden in folgendem Publikationsorgan veröffentlicht:

Al-Maawi S, Vorakulpipat C, Orlowska A, Zrc T, Sader RA, Kirkpatrick CJ, Ghanaati S. In vivo implantation of a bovine-derived collagen membrane leads to changes in the physiological cellular pattern of wound healing by the induction of multinucleated giant cells: An adverse reaction FrontBioengBiotechnol. 2018.

Frankfurt am Main, 30.07.2018

_____

Chakorn Vorakulpipat